Simulated climate and climate change in the GFDL CM2.5 high-resolution coupled climate model

Thomas L. Delworth[1], Anthony Rosati[1], Whit Anderson[1], Alistair J. Adcroft[2], V. Balaji[2], Rusty Benson[1], Keith Dixon[1], Stephen M. Griffies[1], Hyun-Chul Lee[1,3], Ronald C. Pacanowski[4], Gabriel A. Vecchi[1], Andrew T. Wittenberg[1], Fanrong Zeng[1], Rong Zhang[1]

[1] Geophysical Fluid Dynamics Laboratory (GFDL)/NOAA, P.O. Box 308, Princeton University Princeton NJ 08542 USA
[2] Princeton University, Princeton NJ 08542 USA
[3] High Performance Technologies, Inc.
[4] Retired, formerly at GFDL

submitted to Journal of Climate
June 7, 2011

Abstract

We present results for simulated climate and climate change from a newly developed high-resolution global climate model (GFDL CM2.5). The GFDL CM2.5 model has an atmospheric resolution of approximately 50 Km in the horizontal, with 32 vertical levels. The horizontal resolution in the ocean ranges from 28 Km in the tropics to 8 Km at high latitudes, with 50 vertical levels. This resolution allows the explicit simulation of some mesoscale eddies in the ocean, particularly at lower latitudes.

We present analyses based on the output of a 280 year control simulation; we also present results based on a 140 year simulation in which atmospheric CO_2 increases at 1% per year until doubling after 70 years.

Results are compared to the GFDL CM2.1 climate model, which has somewhat similar physics but coarser resolution. The simulated climate in CM2.5 shows marked improvement over many regions, especially the tropics, including a reduction in the double ITCZ and an improved simulation of ENSO. Regional precipitation features are much improved. The Indian monsoon and Amazonian rainfall are also substantially more realistic in CM2.5.

The response of CM2.5 to a doubling of atmospheric CO_2 has many features in common with CM2.1, with some notable differences. For example, rainfall changes over the Mediterranean appear to be tightly linked to topography in CM2.5, in contrast to CM2.1 where the response is more spatially homogeneous. In addition, in CM2.5 the near-surface ocean warms substantially in the high latitudes of the Southern Ocean, in contrast to simulations using CM2.1.

1. Introduction

Climate models are the primary tools for making predictions about the future state of the climate system. It is an important goal of climate science to continually improve these models in order to increase our confidence in the prediction of future climate states. The fidelity and utility of climate models are limited in several key respects, including: (1) incomplete knowledge of the physical, chemical and biological processes that govern the behavior of the climate system, and (2) constraints on computational resources that limit the ability both to simulate small scale processes (such as atmospheric convection and clouds) and to simulate climate on regional spatial scales. This latter limitation is especially troublesome, since it is on these smaller spatial scales that climate change information is oftentimes most needed.

Here we present simulated climate and climate change from a newly developed climate model of much finer resolution than previous climate models used at NOAA's Geophysical Fluid Dynamics Laboratory (GFDL). The improved representation of some smaller-scale processes in the climate system appears to substantially improve the simulation of many key aspects of climate, and is thus an important advance. The present work builds on, and is complementary to, efforts at other institutions to build high-resolution coupled models. For example, Shaffrey et al. (2009) present results from a Hadley Centre model, in which the ocean has a $1/3^{o}$ horizontal resolution and the atmosphere has a horizontal resolution of approximately 1 degree. Their results show significant improvements in simulating many aspects of the climate system. Similarly, Gent et al (2010) show improvements in the mean state from a version of the NCAR CCSM with atmospheric resolution of 0.5 degree. In particular, regional precipitation patterns and their associated river outflows are more realistic than in a coarser resolution version. Sakamato et al. (2012) also show improvements with a high resolution coupled model, especially for orographic effects and coastal upwelling.

2. Model formulation

The model development documented in this paper started from the GFDL CM2.1 climate model (Delworth et al., 2006, hereafter referred to as D06) that was widely used and analyzed as part of the IPCC Fourth Assessment Report (IPCC AR4). This model is still widely used, and output from a large set of experiments is freely available at http://nomads.gfdl.noaa.gov/CM2.X/. The aim of the current effort is to assess how simulations of climate variability and change are altered when the model horizontal resolution is substantially increased, and physical and numerical formulations consistent with that resolution are employed. This grid refinement permits both simulation of phenomena on smaller spatial scales, and improved representation of physical processes in the climate system that operate on smaller spatial scales. We refer to this new higher-resolution model as GFDL CM2.5v1 (where the "v1" denotes that this is "version 1" of this model; we will refer to this model as simply CM2.5 in the remainder of this paper, with the "v1" implicit).

One goal of this model development was to construct a model that had very different characteristics than our previous models, and was effectively in a new part of the "parameter space" of global coupled climate models. For the ocean component of the coupled model we made a conscious decision to build a model that had no explicit lateral diffusion, used viscosity that was as small as numerically possible, and used a highly accurate formulation for advection (see below) that minimizes numerical diffusion. The combination of these factors allows the model to simulate very energetic oceanic flows, including intense boundary currents. We also chose not to use a parameterization of the effects of oceanic mesoscale eddies in this first version of the CM2.5 model, but rather to allow the model to try to simulate eddies explicitly. Although the grid resolution of CM2.5 (discussed below) is insufficient to fully resolve oceanic eddies, especially at higher latitudes, we chose this model development pathway in order to facilitate an assessment of the role of oceanic eddies in the climate system, and to minimize parameterized processes. As shown below, the comparison of our CM2.5 and CM2.6 models can shed light on the role of ocean eddies, and will be the subject of future work (the CM2.6 model will be described briefly in section 2f below).

a. Atmospheric Component

The atmospheric component of CM2.5 is derived from the atmospheric component of the GFDL CM2.1 coupled model (Delworth et al., 2006). The horizontal resolution has been refined from roughly 200km in CM2.1 to approximately 50 Km in CM2.5. The atmospheric component is formulated on a "cubed-sphere" grid (Lin, 2004; Putman and Lin, 2007), in which the spherical atmosphere is represented on six sides of a cube. This formulation avoids the numerical problem of the convergence of meridians at the poles and associated filtering, and allows grid boxes of roughly equal area over the globe.

The parameterized atmospheric physics are nearly identical to that described in GAMDT (2004) and D06, with the exception of some tuning of cloud parameters to achieve a radiative balance at the finer spatial resolution. In addition, there are 32 levels in the vertical, as opposed to the 24 levels used in CM2.1. The extra levels are mainly concentrated in the upper troposphere and lower stratosphere.

b. Oceanic Component

The ocean model is substantially different from that used in CM2.1, previously described in D06, Griffies et al (2005), and Gnanadesikan et al (2006). The ocean grid in CM2.5 is considerably finer, with horizontal spacing varying from 28 km at the equator to 8 km at high latitudes, in contrast to the spacing of approximately 100 Km used in CM2.1. In addition, the grid boxes maintain an aspect ratio close to one, in contrast to CM2.1 where the aspect ratio can exceed 2 at high latitudes due to the convergence of the meridians. Both CM2.5 and CM2.1 use a "tri-polar" grid (Murray, 1996), in which there are displaced poles located over northern Canada and Russia to avoid a singularity at the North Pole. The ocean component for both CM2.1 and CM2.5 uses 50 levels in the vertical.

In addition to finer resolution than in CM2.1, the following are characteristics of the ocean component of CM2.5:

- CM2.5 does not use a parameterization for the effects of mesoscale eddies (in contrast to CM2.1, which uses a parameterization as described in Griffies et al (2005) and Gnanadesikan et al, 2006).

- CM2.5 uses a parameterization for the effects of submesoscale, mixed-layer eddies (Fox-Kemper et al., 2010).
- CM2.5 uses a high-order finite volume advection scheme - the piecewise quartic method (PQM). The PQM is based on fifth-order accurate piecewise polynomials and is motivated by the need to significantly improve ocean climate models which require the remapping to be conservative, monotonic and highly accurate (Huynh,1996; White and Adcroft,2008). This scheme is much more accurate and less dissipative than that used in CM2.1.
- There is no explicit lateral diffusion in CM2.5, and there is no prescribed background vertical diffusion.
- Vertical mixing in CM2.5 is determined by the KPP scheme from Large et al (1994), in addition to the coastal tide mixing scheme of Lee et al (2006). In addition, CM2.5 employs the internal tide mixing scheme of Simmons et al. (2004).
- CM2.5 uses the MOM4.1 code (Griffies et al., 2011), and uses a z* vertical coordinate (see the appendix of Griffies et al., 2011).
- CM2.5 uses very low viscosity with the Smagorinsky biharmonic formulation (Griffies and Hallberg, 2000) and a prescribed background viscosity that is enhanced next to western boundaries.
- All straits connecting bodies of water (such as the Atlantic and the Mediterranean) have explicit flow, rather than a parameterized exchange as in CM2.1.

The sum of these changes creates an ocean component in CM2.5 that is far more energetic than the ocean component of CM2.1. The higher order advection scheme, finer horizontal resolution, and lack of explicit diffusion mean that sharp gradients in both the horizontal and vertical are maintained, such as associated with boundary currents and the thermocline (shown below).

c. Land Component

The land model in CM2.5 is called “LM3” and represents a major change over the land model used in CM2.1. LM3 is a new model for land water, energy, and carbon balance. In comparison to its predecessor (the Land Dynamics, or LaD, model (Milly and Shmakin, 2002)), LM3 includes a multi-layer model of snow pack above the soil; a continuous vertical representation of soil water that spans both the unsaturated and saturated zones; a frozen soil-water phase; a parameterization of water-table height, saturated-area fraction, and groundwater discharge to streams derived from standard groundwater-hydraulic assumptions and surface topographic information; finite-velocity horizontal transport of runoff via rivers to the ocean; lakes, lake ice, and lake-ice snow packs that exchange mass and energy with both the atmosphere and the rivers; and consistent, energy-conserving accounting of sensible heat content of water in all its phases. In stand-alone numerical experiments with observation-based atmospheric forcing, LM3 preserves the generally realistic water-balance partitioning of the LaD model; ameliorates some of the deficiencies of the LaD model previously identified; and provides qualitatively realistic estimates of physical variables that are not tracked by the LaD model.

d. Sea Ice Component

The sea ice component used in CM2.5 is almost identical to that used in CM2.1, called the GFDL Sea Ice Simulator (SIS). SIS is a dynamical model with three vertical layers, one snow and two ice, and five ice-thickness categories. The elastic-viscous-plastic technique (Hunke and Dukowicz, 1997) is used to calculate ice internal stresses, and the thermodynamics is a modified Semtner three-layer scheme (Winton 2000). Details of the model formulation and configuration are given in Appendix 1 of D06. The only difference from the sea ice model used in CM2.1 is that the albedos are higher than in CM2.1, and are closer to the central value of observational estimates from Perovich et al (2002). Specifically, the maximum albedo of snow on sea ice increased from 0.80 in CM2.1 to 0.85 in CM2.5, and the maximum albedo of sea ice increased from 0.58 in CM2.1 to 0.68 in CM2.5.

The details of the flow of ice from continental regions into the ocean, including ice shelves and their interaction with the ocean, is beyond the scope of this model. Therefore, CM2.5 incorporates a recently developed parameterization of the effects of icebergs on the coupled climate system (Martin and Adcroft, 2010), in which the movement of snow from the continent into the ocean causes the formation of a statistical distribution of icebergs. These icebergs move away from the coasts, driven by winds and currents, and eventually melt and deposit their fresh water into the ocean, while maintaining a global hydrologic balance. Further details are in Martin and Adcroft (2010).

Even with this iceberg parameterization, one of the model shortcomings is that at this resolution some of the complexity of the coastal regions of Antarctica and Greenland is captured, but the model is not able to fully represent all of the relevant processes. For example, sea ice forms in some of the small semi-enclosed bays on the Antarctic and Greenland coasts. However, the narrowness of the passageways connecting these bays to the open ocean inhibits the movement of this ice to the open ocean where it could melt. The ice in some of these inlets can be effectively trapped, and continues to grow as more ice is formed. This trapping can result in localized growth of sea ice to hundreds meters in a few such isolated bays; this unrealistic growth reflects model limitations.

e. Coupling characteristics and model timesteps

The model ocean and atmosphere exchange fluxes once every hour, and are thus able to represent a diurnal cycle in coupling characteristics. In addition, the surface current speeds are taken into account when computing wind stresses on the ocean (Pacanowski, 1987). The timestep is 20 minutes for most atmospheric physics, but is 3 hours for radiation. The ocean timestep is 30 minutes.

f. Simulations

A number of simulations from both models are examined. For CM2.1 we use the following experiments:

- **CM2.1_1990_Control**: a 300 year simulation with atmospheric composition (greenhouse gases, aerosols) and external forcing (solar irradiance) fixed at 1990 levels.
- **CM2.1_1990_Control_NO_GM**: a 100 year simulation identical to the 1990 Control for CM2.1, except that there is no parameterization of the effects of mesoscale eddies in the ocean.

For CM2.5 we use the following experiments:

- **CM2.5_1990_Control**: a 280 year simulation with atmospheric composition (greenhouse gases, aerosols) and external forcing (solar irradiance) fixed at 1990 levels.
- **CM2.5_2X_CO_2**: 140 year simulation that starts from year 101 of the 1990 control simulation, but in which atmospheric CO_2 increases at a rate of 1% per year until reaching double its initial value after 70 years, and is held fixed thereafter.

When calculating the model's response to doubled CO_2 it is common to start the doubled CO_2 simulation from a long control simulation with 1860 atmospheric composition; such an "1860 Control" simulation produces a climate that may be closer to a radiative balance, since the atmospheric composition is closer to preindustrial conditions. However, such 1860 Control simulations can take many centuries to come into balance, and the CM2.5 model is very computationally expensive. Therefore, we used our 1990 Control simulation as the starting point for the CM2.5 2X CO_2 simulations.

In order to make a clean comparison with CM2.1, we also need a 2X CO_2 simulation of CM2.1 that starts from a 1990 Control simulation. This had not been done previously (the 2X CO_2 simulations with CM2.1 had been done from an 1860 Control simulation), so a new pair of simulations was conducted. However, the computer system had changed since the original CM2.1 simulations were conducted, and thus we were not able to precisely replicate the original CM2.1. In addition, several minor code bugs had been discovered, and those had been corrected. Therefore, for the 2X CO_2 runs with CM2.1, we used a slightly different version of CM2.1 than what we used for the IPCC AR4. This version of CM2.1 also uses values of albedo over sea ice that are higher than the original CM2.1, but identical to CM2.5. This slightly revised version of CM2.1 can be referred to as "CM2.1v2". In this paper we use output from the revised version of CM2.1 to compare the CO_2 responses of CM2.1 and CM2.5, but use the original version of CM2.1 for comparing the time-mean state and most of the internal variability between CM2.1 and CM2.5.

A comparison of the original and new versions of CM2.1 (not shown) confirms that the climates are extremely similar. Further, we also have available a 2X CO_2 run with the original version of CM2.1, but starting from an 1860 control simulation; the response to increasing CO_2 is similar in the original and revised versions of CM2.1. Since the original and revised versions of CM2.1 are extremely similar in both their control simulations and response to CO_2, we still refer to this revised model in the text as CM2.1.

Therefore, for estimating the response of CM2.1 to a doubling of CO_2, we use the following experiments that were conducted with the revised version of CM2.1:

- **CM2.1_1990_Control**: a 240 year simulation with atmospheric composition (greenhouse gases, aerosols) and external forcing (solar irradiance) fixed at 1990 levels.
- **CM2.1_2X_CO_2**: 140 year simulation that starts from year 101 of the 1990 control simulation, but in which atmospheric CO_2 increases at a rate of 1% per year until reaching double its initial value after 70 years, and is held fixed thereafter.

We will also make use of an additional prototype higher resolution climate model, GFDL CM2.6. This model has the same atmosphere as CM2.5, and identical ocean physics as CM2.5. The CM2.6 ocean component has substantially higher horizontal resolution than CM2.5, with grid spacing varying from 11 Km at the equator to less than 4 Km at very high latitudes. As shown below, the CM2.6 model simulates a very realistic distribution of ocean eddy activity. Due to the computational expense of this model we have only performed a 30-year 1990 control simulation, but the comparison with CM2.5 helps to illuminate some of the physical factors responsible for the biases present in CM2.5, with particular emphasis on the role of ocean eddies.

To derive the ocean initial conditions for the 1990 control integration, a one-year integration of the ocean component of the coupled model (CM2.1, CM2.5, or CM2.6) is conducted starting from observed climatological conditions (taken from Steele et al., 2001, which is an extension of Antonov et al (1998) and Boyer et al (1998)), with the ocean initially at rest. The ocean model is forced with surface fluxes (Griffies et al., 2009); in addition, surface temperature and salinity are restored to the Steele et al. (2001)

climatology with a 10-day restoring time scale. The purpose of the one-year run is to avoid initializing the coupled model with an ocean at rest. Output from the end of that one-year spin up is taken as the initial condition for the coupled run. The atmospheric initial conditions are taken from the end of an atmosphere-land simulation with prescribed SSTs.

3. Simulation characteristics

a. Model drift

We first examine the temporal drift of the 1990 control simulations. Shown in Fig. 1a are the time series of the annual mean, global mean net radiation at the top of the atmosphere. For both models there is a rapid initial increase to slightly more than 1 W m^{-2}, after which there is a slow decline over the following centuries (positive values indicate more radiation entering the Earth's climate system than exiting to space). This imbalance is reflected in a long-term increase in oceanic heat content.

Shown in Figure 1b are the time series of annual mean, global mean surface air temperature. For both models there is an initial cooling over the first several decades, with greater cooling in CM2.5 than CM2.1. As discussed below, part of this initial cooling appears to be related to a model bias in which heat is pumped from the near-surface ocean layers into the interior ocean. The movement of heat away from the ocean surface leads to surface cooling, which is then amplified by cloud feedback; the cooler surface waters increase low level cloudiness, resulting in increased reflection of shortwave radiation to space and further cooling. On somewhat longer time scales there is a slow warming trend, related to the positive radiative imbalance and the overall warming of the ocean.

Shown in Figure 2 are the maps of SST bias, computed as the annual mean simulated SST over years 101-200 of the 1990 Control Simulations minus observed (positive values indicate that the simulated SST is larger than observed; the observed data is described in Smith et al, 2008). The overall pattern of bias is similar between the two models, although the global mean temperature in CM2.5 is lower than in CM2.1, and this is reflected in Figure

2 as well. A prominent bias remains in the simulation of the North Atlantic current east of Newfoundland, with a large cold bias in both models, but larger in CM2.5. The warm bias in the Southern Ocean is reduced in CM2.5. One notable improvement in CM2.5 relative to CM2.1 is the near elimination of the positive SST biases off the west coast of South America and the southwest coast of North America. However, the overall root mean square error (RMSE) of simulated SST is similar between the two models (1.17K in CM2.1, 1.25K in CM2.5).

Drifts in the ocean interior are shown in Figure 3. In both models a cold bias develops in the upper two hundred meters, with a warm bias below that, and a maximum warm bias around 500-900 meters depth. The overall warming signal is consistent with a positive radiative imbalance at the top of the atmosphere, with the net heat gained in the climate system being stored in the ocean interior. An important difference is that both the subsurface warming and the near-surface cooling are much larger in CM2.5 than in CM2.1; this aspect is discussed below.

The pattern of subsurface warming has maxima in the regions of the subtropical gyres (not shown), at depths from 500-900 meters. This suggests that the warming drift may be related to subduction associated with the subtropical gyres. A hypothesis for this drift is as follows: once the simulation starts, wind-driven subduction in the subtropical gyres deepens the thermocline, leading to the subsurface warming; this continues until other processes are strong enough to balance that deepening. We hypothesize that lateral heat transport by ocean mesoscale eddies is an important part of this balance, and that insufficient transport by eddies allows the thermocline in the models to deepen more than observed in Nature; this leads to the subsurface warming drift. As the subtropical gyres deepen, the increased horizontal gradients should enhance mesoscale eddy activity, thereby enhancing the lateral transport of heat away from the gyres and inhibiting further deepening of the gyres and the subsurface warming. We hypothesize that in the absence of sufficient eddy heat transport (whether through explicitly resolved eddies or a parameterization of their effects), the thermocline in the subtropical gyres continues to deepen, implying continued movement of heat from the near-surface layers to the interior thermocline; this will result in the cool bias seen in the upper several hundred meters and the warm bias below.

The above hypothesis is consistent with the fact that the drift is larger in CM2.5, which does not parameterize the effects of mesoscale eddies, than in CM2.1, which includes such a parameterization. We test this hypothesis by conducting a simulation of CM2.1 that is identical to the 1990 Control simulation described previously, but does not use a parameterization of mesoscale eddies. This new experiment is called "CM2.1_1990_Control_NO_GM". The hypothesis predicts that the subsurface drift in this new experiment should be considerably larger than in the standard control run of CM2.1, since there are no eddy effects to inhibit the deepening of the subtropical gyres. Results (not shown) from this additional simulation support the hypothesis, with the drift in the new run increased by almost a factor of two. The largest increase in subsurface warm biases are in the subtropical gyres, also consistent with the hypothesis.

We can further test this hypothesis by using the CM2.6 model, which has the same atmosphere as CM2.5 but uses a much finer resolution in the ocean. The CM2.6 model is computationally expensive to run, but we have conducted a 30-year simulation using the same forcings as the 1990 Control simulation of CM2.5, and using similar initial conditions as CM2.5. The above hypothesis predicts that CM2.6 should have a much smaller subsurface drift than CM2.5, since the much finer grid in CM2.6 will permit substantially enhanced eddy activity that should serve to moderate the deepening of the subtropical gyres. It will be shown later (see Fig. 12) that CM2.6 does indeed have much larger values of eddy kinetic energy in the ocean, consistent with a much more vigorous mesoscale eddy field, and closely resembling observational analyses. We show in Figure 4 that when we have a very active eddy field, as in CM2.6, the subsurface drift is reduced by a factor of 3 or more relative to that in CM2.5. The near-surface cooling is also substantially reduced. This result using CM2.6 provides very strong support that the subsurface drift present in CM2.5 is largely attributable to insufficiently resolved mesoscale eddies in the ocean, combined with the lack of any parameterized eddy effects. This result is also a clear demonstration of the significant role that ocean mesoscale eddies may play in the climate system.

b. Time-mean surface climate characteristics

We now wish to examine some of the time-mean simulation characteristics from the CM2.5 1990 Control simulation. As a first assessment, we use near-surface air temperature and precipitation as simulated by the model to construct maps of Koppen climate classifications for both CM2.1 and CM2.5, and compare those to observations (see, for example, Kottek et al, 2006; Gnanadesikan and Stouffer, 2006). The Koppen climate classification system uses the seasonal cycles of temperature and rainfall at a continental location to characterize that location as belonging to one of a set of previously defined climatic types. These include classifications such as tropical rainforest, savanna, desert, and polar. We calculate the percentage of continental areas in which the simulated Koppen climate classification type is different than observed. For CM2.1 this number is 23%, whereas for CM2.5 this number is 17%, a reduction in relative error of 26%. While there are widespread improvements, the largest improvements come from South America, where CM2.5 simulates substantially more rainfall over the Amazon basin. This demonstrates the substantial improvement of mean continental climate in terms of the seasonal cycles of temperature and precipitation for CM2.5 versus CM2.1.

We next examine precipitation as simulated over several continental regions. Shown in Figure 5 is annual mean precipitation over North America from CM2.1, CM2.5, and a land-only observational data set (Legates and Wilmott, 1990; updated data available at http://climate.geog.udel.edu/~climate/html_pages/precip_clim.html). There is a marked improvement in CM2.5 relative to CM2.1. Much of this improvement is likely attributable to the refined representation of orography in CM2.5, particularly over the western U.S. For example, the precipitation maximum associated with the Sierra Nevada Mountains becomes apparent in CM2.5. However, there is generally too much rainfall over the western U.S. in CM2.5 compared to observations. The observed structure of the east-west gradient of precipitation over the U.S. Midwest is also more apparent in CM2.5, although the gradient is not as sharp as in the observations.

Shown in Figure 6 is annual mean precipitation over Europe from observations (Legates and Wilmott, 1990), CM2.1 and CM2.5. Similarly to North America, there is a significant improvement in precipitation in CM2.5 relative to CM2.1, likely associated with refined orography. For example, the structure of simulated precipitation over the United Kingdom is much improved in CM2.5 relative to CM2.1, with local maxima along the west coasts of Scotland and Ireland as in the observations. Similar improvements are clear over many other regions, including the coast of Norway and the Iberian peninsula.

Shown in Figure 7 is precipitation over India and surrounding regions for the months of June-September (the monsoon season). We show results from two observational data sets (the satellite-based TRMM dataset and a station based dataset) to provide a perspective on observational uncertainty in precipitation estimates in this region. CM2.5 shows notable improvement in simulated precipitation relative to CM2.1, a model which was found to have a realistic simulations of South Asian monsoonal climate relative to the IPCC-AR4 models (*e.g.,* Annamalai *et al.* 2007, Rajeevan and Nanjundiah 2010). In particular, the two separate maxima in precipitation (one in Western Ghats along the west coast, the other in the Gangetic Plain to the north east) are captured realistically, as is the arid region in southern India and just off the southeast coast, although not as intense as observed. The structure of the rainfall maximum over the Bay of Bengal is improved, with more rainfall in the eastern portion of the Bay, but the amount is still substantially less than observed. These results suggest that going to even finer resolution could yield further improvements.

Zonally averaged rainfall over the eastern tropical Pacific is shown in Figure 8. The tendency for a double ITCZ (Intertropical Convergence Zone) in CM2.1 is reduced in CM2.5, and the position of the rainfall maximum to the north of the equator is in better agreement with observations. These improvements are also visible in Figure 9, which shows maps of simulated and observed tropical rainfall. Rainfall in the eastern Pacific is reduced south of the equator in CM2.5, bringing the CM2.5 model in closer agreement with observations. There is an overall tendency for rainfall over the oceans to be more intense than observed. Rainfall over the Amazon improves significantly in CM2.5 relative to CM2.1, although it is still smaller than observed. The improved land model employed in CM2.5 may have helped in this region.

A factor contributing to the overall improvement of tropical precipitation, especially in the eastern Pacific, appears to be an improved representation of the Andes Mountains in South America and regional wind-stress patterns, as well as small-scale oceanic features, including upwelling off the west coast of South America. Shown in Figure 10 are maps of SST and the vertical structure of ocean temperature in this region from CM2.1, CM2.5, and an observational data set (Antonov et al., 1998). It is clear that the coarse resolution model (CM2.1) does not simulate the cool ocean temperature adjacent to the coast of South America between 5^{o}S and 20^{o}S, whereas CM2.5 appears to capture this feature, and bears a closer resemblance to the observations (compare Figure 10a-c). The cross sections of ocean temperature (Fig. 10,d-f) demonstrate that relatively cool subsurface waters reach the surface in the observations and CM2.5, but not in CM2.1. There is a warm layer of near-surface water in CM2.1 close to the coast. These results suggest (and additional analyses, not shown, confirm) that coastal upwelling in CM2.5 is more vigorous, bringing cooler subsurface waters to the surface, resulting in the cool surface waters near the coast (see also Gent et al., 2010). This process appears to have a larger scale influence, as the cool surface waters move northwestward with the mean surface currents, thereby cooling the surface water to the south of the equator in the eastern tropical Pacific. This distribution of SST tends to favor a single ITCZ north of the equator, instead of the double ITCZ seen in CM2.1 where there is also warm water south of the equator. These improvements in the representation of small-scale processes then have influence on a much larger scale. It is clear that CM2.5 still has a double ITCZ, but it is improved relative to CM2.1.

c. Large-scale ocean circulation characteristics

The ocean circulation is far more energetic in CM2.5 than in CM2.1. Shown in Figure 11 are maps of the time-mean ocean surface velocities in CM2.1 and CM2.5 for parts of the North Atlantic. The finer resolution, lower viscosity, higher order advection scheme, and lack of explicit lateral diffusion used in CM2.5 permit the model to simulate much higher velocities, especially in the vicinity of the boundary currents. For example, the largest annual mean northward current speed off the east coast of Florida is 1.42 m s^{-1} in CM2.5, compared to 0.37 m s^{-1} in CM2.1. The boundary currents also have much tighter and less diffusive structures. Compare, for example, the boundary flows around the periphery of the Labrador Sea in both models.

Shown in Figure 12 are maps of the Eddy Kinetic Energy (EKE) in the models and derived from satellite observations. The map of EKE in observations (Fig. 12a) shows a rich structure, with large EKE in boundary currents and some interior regions. The coarse resolution of CM2.1 does not permit the formation of eddies, with the exception of the deep tropics, and the EKE amplitude in CM2.1 is thus very small (Fig. 12b). The EKE field is more realistic in CM2.5 (Fig. 12c) than in CM2.1, as to be expected from the finer resolution and lower viscosity. The magnitude of the EKE in CM2.5 is still, however, somewhat below that observed, suggesting that still finer ocean resolution is needed to fully capture eddy kinetic energy. This point is confirmed when examining EKE in CM2.6 (Fig. 12d) which is in excellent agreement with observational estimates.

The structure of the time-mean Atlantic Meridional Overturning Circulation (AMOC) is shown in Figure 13 for CM2.1 and CM2.5 (the definition of this field is described in the Figure caption). The overall transport is reduced in CM2.5 relative to CM2.1. At 26.5^{o}N, the AMOC in CM2.5 is 14.4 Sverdrups (Sv; 1 Sv = 10^6 m^3 s^{-1}) versus 18.1 SV in CM2.1; the most recent observational estimate of the AMOC at 26.5^{o}N is 18.5 SV (Johns et al., 2011; Kanzow et al., 2010). The total poleward oceanic heat transport in the North Atlantic in CM2.5 peaks at about 10^{15} Watts (1 PW), similar to CM2.1, but less than recent observational estimates of 1.3 PW (Johns et al., 2011).

We speculate that insufficiently resolved overflows of dense water through the Denmark Straits and Faroe channels may contribute to this somewhat weak North Atlantic heat transport. In a separate sensitivity test using CM2.5 with deepened topography downstream of the Denmark Straits (see Zhang et al., 2011, for details), the outflow of dense water from the Nordic Seas was significantly enhanced, resulting in a deepening of the AMOC by about 1000 m. There was also an increase in the total oceanic heat transport in the North Atlantic from 0.96 PW to 1.13 PW at 26.5^{0}N, and the AMOC at 26.5^{0}N increased from 15 Sv to 18 Sv. However, these results were based on 5-year means from a short sensitivity test, and they need to be confirmed with additional sensitivity tests. They do suggest, however, that deficiencies in the representation of overflows may contribute to this bias. This issue is discussed further in section 4c below.

In the Southern Hemisphere, the Antarctic Circumpolar Current (ACC) is a major feature of the oceanic circulation in high latitudes. One measure of this flow, defined as the total zonal oceanic volume transport through 82^{o}W between Antarctic and South America, from the surface to the bottom of the ocean, has a time-mean value of 116 Sv in the CM2.5 Control simulation. This is somewhat smaller than the value of 130-140 Sv found in CM2.1 (see Fig. 9 of D06), and smaller than observational estimates of 135 Sv (Cunningham et al, 2003), although the uncertainty associated with the observational estimates can be significant. After an initial weakening in the control simulation, the circulation is fairly steady, with modest variability (not shown).

d. Sea Ice

There is a change in the simulation of annual mean sea ice thickness between CM2.1 and CM2.5, as shown in Fig. 14 (panels a and b). In the Arctic, the sea ice in CM2.5 is substantially thicker than in CM2.1, with maximum sea ice values near the Canadian coast and archipelago. The increase in albedo between CM2.1 and CM2.5 (see section 2d) is a substantial contributor to the thicker (and more realistic) sea ice in CM2.5. Improved atmospheric circulation (not shown) also helps to create the drift stream of sea ice from Siberia to the Canadian archipelago. This feature is more diffuse in CM2.1. A similar improvement in sea ice relative to CM2.1 is also seen in the GFDL CM3 coupled model (Griffies et al., 2011).

There is also an increase in sea ice thickness in the Southern Hemisphere (Figure 14, panels c and d), with very large values in small-scale bays and inlets (these are also seen in the Northern Hemisphere). As mentioned briefly in section 2d, the fine resolution allows the model to include many small bays and inlets. In such regions, the flow of snow and ice into the ocean is a complex process, including such factors as ice shelves and grounded ice sheets. The model is not able to satisfactorily represent such small-scale processes. One of the consequences is that sea ice can be formed in such restricted areas as snow builds up in continental regions and "runs off" (calves) into the small bays and inlets. However, the rate at which this new ice forms is sometimes greater than the rate at which the model is able to move such ice into the open ocean where it can melt. As a result, ice can grow unrealistically thick in such regions (to hundreds of meters). This points to a need for improved representation of such coastal ice processes in future high-resolution models. The problem is much less severe at coarser resolutions where the connection of coastal regions to the open ocean is less restricted.

e. ENSO

Previous work has described the tropical climate and ENSO in CM2.1 (Wittenberg et al. 2006; Wittenberg 2009; Kug et al. 2010). Here we focus on how CM2.5's tropical variability and ENSO compare with observations and CM2.1.

The spatial patterns of tropical interannual SST variability are shown in Fig. 15 (observations from Smith et al., 2008; model diagnostics of ENSO-related variability in Figures 15-17 use the full length of the experiments). CM2.1_1990 exhibits strong equatorial Pacific variability (ENSO), stronger than that observed in recent decades. Both CM2.1_1990 and CM2.5_1990 place the center of Pacific SSTA variability west of the observed pattern, with too little variability along the coast of Peru; both are common biases among CGCMs (Guilyardi et al. 2009). However, CM2.5 agrees more closely with observations than CM2.1, with a weaker Pacific ENSO (especially west of the dateline) and weaker interannual variability of Indian Ocean SSTs. Within the tropics, only the Atlantic shows stronger interannual SSTA fluctuations in CM2.5 than CM2.1. With CO_2 doubling, both models show a slight increase in tropical interannual SST variability (not shown).

Fig. 16 shows time-mean spectra of NINO3 SSTs for the models and observations. All three time series exhibit interdecadal modulation of the ENSO amplitude and period, producing a broad spectrum in the interannual band. The interdecadal modulation of ENSO poses challenges for evaluating models using short observational records, and for assessing the future of ENSO (Wittenberg 2009; Vecchi and Wittenberg 2010; Collins et al. 2010). Yet it is clear that the CM2.1 spectrum is stronger than observed at semiannual and interannual time scales -- a difference detectable even with time series as short as 20 years. In comparison with CM2.1, the CM2.5 spectral power is generally weaker and more consistent with observations, except at periods near 2-2.5 years where the CM2.5 spectrum peaks.

The seasonal cycle of tropical SST has weakened slightly in CM2.5 relative to CM2.1, which represents an improvement relative to observations. The largest attenuation is near the coast of Peru, where both the SST and southeasterly wind seasonal cycles have weakened in CM2.5 (not shown). The cause may be CM2.5's weaker upper-ocean thermal stratification near South America, as seasonal wind anomalies and their associated upwelling (linked to the seasonal migration of the ITCZs) tap into a weaker subsurface contrast and thereby generate weaker seasonal SST changes. The reduced seasonally-alternating ITCZ in CM2.5's eastern tropical Pacific, and associated reductions in the semiannual cycle of equatorial wind speed and evaporation, have also weakened the semiannual cycle of NINO3 SST -- again bringing CM2.5 more in line with observations.

The shorter ENSO period in CM2.5 may be linked to a change in the structure of the wind stress response to SSTAs (not shown). Compared to CM2.1, in CM2.5 the equatorial westerly wind stress anomalies that develop near the dateline during warm events are meridionally narrower and more trapped in the west, especially on their southern flank. Studies have shown that models with narrower or westward-shifted westerly anomalies tend to exhibit weaker ENSOs with shorter periods (Kirtman 1997; An & Wang 2000; Wittenberg 2002; Capotondi et al. 2006; Kim et al. 2008). This change occurs because of increased cyclonic wind stress curl close to the equator and western boundary during warm events, which shortens the time needed for the off-equatorial oceanic Rossby wavetrain to reflect at the western boundary as equatorial Kelvin waves. This shorter time for wave reflection more rapidly reverses the sense of zonal advection along the equator, and also more rapidly establishes a poleward Sverdrup transport which discharges upper-ocean heat content from the equator. Both effects contribute to faster termination of warm events in models with meridionally narrower or westward-shifted Pacific zonal wind stress anomalies. The narrower zonal wind stress anomalies in CM2.5 may themselves result from the meridionally narrower rainfall anomalies in that model, linked to the equatorward-shifted climatological ITCZs (see Fig. 8).

Another factor behind the attenuation of ENSO in CM2.5 versus CM2.1 is stronger damping of SSTAs by surface heat fluxes in CM2.5 (not shown). For CM2.5 warm events, there is a larger cloud-shading response in the central Pacific (as deep convection shifts farther east than in CM2.1), and also in the east Pacific (as ITCZ deep convection shifts farther equatorward than in CM2.1). In CM2.5 there is also more evaporative cooling during warm events. This increased cooling is due to higher SSTs and drier surface air in the mean state, which make evaporation more sensitive to SSTAs than in CM2.1; and also to more anomalous warming of SST and drying of surface air in the eastern equatorial Pacific during CM2.5's warm events, which further increases evaporative damping of SSTAs.

Fig. 17 shows the boreal winter response of northern extratropical circulation to ENSO. As described in Wittenberg et al. (2006), CM2.1 exhibits 200-hPa geopotential height extrema that are weaker than and displaced 20°-30° west of those observed -- due in part to similarly westward-shifted responses of the equatorial SST and rainfall. While the North Pacific low and Canadian high remain displaced somewhat westward from their observed positions in CM2.5, there are also significant improvements in the extratropical response. The extrema over the North Pacific and Canada have strengthened, the Pacific low extends farther northwestward towards Siberia , the low over the southeastern United States has become a distinct center, and the low over southeastern China has weakened.

4. Response to increasing CO_2

We next assess the sensitivity of the CM2.1 and CM2.5 models to increasing CO_2. As described in section 2f, we have completed simulations in which CO_2 increases at a rate of 1% per year until reaching double its initial concentration after 70 years, and is then held constant for the remaining 70 years of the simulation. The complete climate system, especially the deep ocean, will not come into equilibrium over this time scale, and so we are examining aspects of the transient response. Note that as described in section 2f we use a slightly modified version of CM2.1 for the 2X CO_2 simulations, and this can be referred to as CM2.1v2. However, since the simulations of CM2.1 and CM2.1v2 are extremely similar, and their response to increasing CO2 are also very similar, for convenience we shall still refer to this slightly revised version of the model as CM2.1. The essential conclusions as described are similar for CM2.1v2 and CM2.1 (as evaluated from a 2X CO_2 simulation starting from an 1860 control simulation).

a. Transient response

Shown in Fig. 18a are the time series of global mean, annual mean near-surface air temperature changes in response to increasing CO_2. The response is computed as the simulated values in the 2X CO_2 experiments minus corresponding values from the control simulations. It is clear that both the rate of warming and the total warming in CM2.5 are somewhat larger than in CM2.1. Since the atmosphere-land component of CM2.5 differs somewhat from CM2.1, especially with regard to the land model used, it is not clear to what extent the different response reflects different physics versus different resolution. Shown in Fig. 18b are time series of global mean, volume mean temperature changes in response to increasing CO_2. The oceanic rate of heat uptake in CM2.5 is slightly larger than in CM2.1 for the first 70 years, but appears similar thereafter. Thus, both the ocean and the near-surface atmosphere are warming somewhat more rapidly in CM2.5 than in CM2.1 for the first 70 years. The transient climate response (global mean temperature change at the time of CO_2 doubling) is approximately 1.6K in this version of CM2.1 and 2.0K in CM2.5. Further work will be necessary to evaluate whether the higher resolution in CM2.5, especially in the ocean where eddies may have important effects, plays any role in the differing response to CO_2.

b. Patterns of change

The spatial pattern of the near-surface air temperature change in response to increasing CO_2 is shown in Fig. 19, which shows the annual mean, time-mean differences between the 2X CO_2 runs and their respective controls for years 91-140 (year 91 is 20 years after CO_2

has reached twice its initial value). The larger overall warming in CM2.5 is readily apparent, with maximal warming at high latitudes of the Northern Hemisphere.

Several differences are noteworthy. In the North Atlantic there is more warming in CM2.5 than in CM2.1. As will be discussed below, there is a smaller reduction of the AMOC in response to increased CO_2 in CM2.5 than in CM2.1, and hence the poleward oceanic heat transport reduction is smaller in CM2.5. The reduced poleward oceanic heat transport in CM2.1 offsets a large part of the warming in the subpolar North Atlantic in CM2.1. In contrast, the ocean heat transport reduction in CM2.5 is much smaller, and is thus not able to offset the CO_2 induced warming, resulting in a larger warming in the subpolar North Atlantic in CM2.5.

There is a very notable difference in the high latitudes of the Southern Hemisphere, with much greater near-surface warming poleward of 45^{o}S in CM2.5 than in CM2.1. The relative minimum in warming in CM2.1 in those latitudes is a common feature of many models, and has been shown to be associated with strong oceanic heat uptake in the Southern Ocean (Meehl et al, 2007, see Fig. 10.8; Flato and Boer, 2001; Manabe et al, 1991). This uptake distributes the warming over a deep vertical section of the Southern Ocean, thereby diminishing the amplitude of surface warming. In contrast, there is strong near-surface warming in the high latitudes of the Southern Hemisphere in CM2.5. The subsurface ocean in CM2.5 for this region is not taking up as much heat as in CM2.1. This is shown in Fig. 20, which shows subsurface temperature changes in CM2.5 and CM2.1. The larger penetration of heat in the high latitudes of the Southern Ocean in CM2.1 is readily apparent.

There are at least two possible explanations for this difference. One possibility is that the mean ocean state of CM2.5 in the high latitudes of the Southern Ocean is more stable in the vertical than CM2.1, thereby inhibiting convection and keeping the warming signal near the surface. This stability may arise from processes that have nothing to do with oceanic resolution. Another possibility is that the presence of oceanic eddies significantly modifies the oceanic response to external perturbations. Previous work with an earlier version of a closely related model with similar oceanic resolution (GFDL CM2.4; Farneti et al., 2010;

Farneti and Delworth, 2010) as well as a high-resolution ocean-only model (Hallberg and Gnanadesikan, 2006) shows that the response of the Southern Ocean circulation to enhanced zonal wind stress can be much different when oceanic eddies are present. Enhanced westerly winds in the Southern Ocean induce a northward Ekman transport of near-surface waters, and a steepening of the isopycnals. Farneti et al (2010) show that in a high-resolution model, the enhanced winds lead to enhanced eddy activity, and that changes in poleward eddy fluxes partially compensate for the enhanced equatorward Ekman transport, leading to weak modifications in local isopycnal slopes. Thus, the response to the enhanced westerly winds is greatly modified and moderated by the presence of oceanic eddies. There exists the possibility that eddies in CM2.5 could modify the response to CO_2. A complete explanation for the differences in the Southern Ocean warming is beyond the scope of this paper. However, there is a pronounced lack of ventilation of the deep ocean in the Southern Hemisphere (not shown) in CM2.5 that appears to be inconsistent with some observational results. Therefore, it is quite possible that the relatively large near-surface warming in the high southern latitudes of CM2.5 is related to the mean state stratification. Future work will examine more carefully the reasons for the relatively large near-surface warming in CM2.5 relative to CM2.1.

The map of annual mean precipitation changes in response to increasing CO_2 is shown in Fig. 21. The broad patterns of enhanced rainfall in parts of the deep tropics, along with high latitudes, and a reduction of precipitation in the subtropics is similar between CM2.1 and CM2.5; this meridional banding of the precipitation response in CM2.5 corresponds to the "wet get wetter/dry get drier" pattern that is a robust response across IPCC-AR4 climate models (Held and Soden 2006). There are some notable differences, however. For example, while CM2.1 has substantial rainfall reductions over the Sahel (see Held et al., 2005), such reductions are small in CM2.5. There are also larger rainfall reductions over tropical regions of South America in CM2.5 than in CM2.1.

There are substantial differences in projected precipitation changes over southern Europe and the Mediterranean, as shown in Fig. 22 (b and d). There is a broad area of precipitation reduction over southern Europe and the Mediterranean in CM2.1, consistent with many models used in the IPCC AR4 report (se Figs. 10.9 and 10.12, Meehl et al., 2007). In contrast, the reductions in rainfall in CM2.5 are somewhat smaller, are tightly associated with topography, and are largest over mountainous terrain. This represents a different projection of possible rainfall changes over southern Europe and the Mediterranean, and would have a fundamentally different societal impact. Further analysis and experimentation is needed to more thoroughly understand why these precipitation projections differ so substantially between the models, and which is more credible. There are also differences in model projections of precipitation changes over North America (Fig. 22a and 22c), and their significance and causal factors need to be more carefully examined in future work.

In response to CO_2 doubling, CM2.5 has an enhanced warming of eastern equatorial Pacific surface temperature (Fig. 19), an eastward shift of equatorial Pacific precipitation (Fig. 21), and a weakening of the Pacific Walker circulation (not shown); these precipitation and Walker Circulation responses in CM2.5 are also present in most IPCC-AR4 models (*e.g.*, Vecchi and Soden 2007, Vecchi and Wittenberg 2010, Collins *et al.* 2010). Though the tropical Pacific response appears "El Niño-like", the western North American precipitation response to CO_2 doubling in CM2.5 deviates substantially from that typically associated with El Niño (Fig. 22c): the drying in Southwestern North America and wet conditions in the Pacific Northwest are typical of La Niña conditions (*e.g.,* Larkin and Harrison 2005). In addition, although the tropical Pacific surface temperature and precipitation response of CM2.5 to $2xCO_2$ is more "El Niño-like" in its structure than that of CM2.1 (Figs. 19, 21), the precipitation response over North America is more "La Niña-like" in CM2.5 than in CM2.1. These model responses and other recent studies (*e.g.*, Collins 2005, Vecchi and Soden 2007, DiNezio et al. 2010) highlight how El Niño provides an incomplete (possibly misleading) analogue for interpreting the character of and mechanisms behind the climatic response to changing radiative forcing.

c. Atlantic Meridional Overturning Circulation

Time series of the AMOC for CM2.1 and CM2.5 are shown in Figure 23 for both the 1990 Control simulations and the 2X CO_2 simulations. The AMOC in CM2.1 has substantial interdecadal variability with a timescale of approximately 20 years; in contrast, interdecadal AMOC variability in CM2.5 is rather muted. One hypothesis for this muted interdecadal variability involves a pronounced bias in mixed layer depths in the Labrador Sea where the water is much less stratified than in observations. As a result, convection to depths greater than 3000 meters occurs each year in CM2.5, with little interannual variability. This continual deep mixing and lack of interannual variability may serve to mute any AMOC variability and sensitivity to perturbations, since variability and change in Labrador Sea convection is thought to be an important factor in AMOC decadal variability and change (see, for example, Boning et al., 2006). There is substantial multidecadal variability in the Greenland, Iceland and Norwegian Seas in CM2.5, but this signal of variability is not communicated to the North Atlantic.

There are at least two potential reasons for this persistent deep mixing in the Labrador Sea in CM2.5: (1) With no parameterization of the effects of ocean eddies in CM2.5, and with insufficient horizontal resolution to fully resolve eddies in the Labrador Sea, there is relatively weak eddy mixing of the fresh water in the boundary current into the interior of the Labrador Sea. Such transport would help to stratify the Labrador Sea and reduce convection. (2) As described previously, the resolution of the model is not sufficient to fully represent the flow of dense water over the Denmark Straits and into the deep layers of the Labrador Sea (Winton et al., 1998). This bias leads to warmer and lighter water at depth than observed, also serving to destabilize the water column and enhance wintertime convection. In order to partially address this bias, a new version of CM2.5 is being developed in which the Denmark Strait and Faroe Bank channel overflows are parameterized using a formulation developed as part of the NOAA/NSF funded US Climate Process Team [Danabasoglu et al, 2010]. Preliminary experiments with this parameterization in both CM2.1 and CM2.5 have shown that it leads to an increase in the amount of cold, dense water in the deeper layers of the Labrador Sea (below 2000 meters). There is also a significant reduction in Labrador Sea convection, as measured by mixed layer depth. It is anticipated that this parameterization will be employed in a new version of CM2.5 under development.

The reduction of the AMOC in response to increasing CO_2 is somewhat smaller in CM2.5 than in CM2.1, dropping from a mean of around 16 Sv to a little under 14 Sv, for a reduction of approximately 15%. The AMOC in CM2.1 drops from around 20 Sv to about 16 Sv, a reduction of approximately 25%. The smaller AMOC reduction in CM2.5 may be related to the tendency for strong convective mixing each winter in the Labrador Sea (discussed in section 3c). In CM2.1 the upper ocean warming and freshening in response to increasing CO_2 increases the stratification in the Labrador Sea, thereby reducing convection and weakening the AMOC. The persistent bias in CM2.5 appears to be able to maintain a greater degree of convection, and thus the AMOC reduction is smaller. A more detailed analysis of the differences in AMOC response to increasing CO_2 is beyond the scope of this paper.

5. Summary and discussion

Improving climate models so that they can provide more robust and credible projections of climate change and variability, particularly on the regional scale, is a critical goal in climate science. Towards this goal, we have presented an overview of the model components and simulation characteristics of the GFDL CM2.5 global coupled model. This model is a descendant of the GFDL CM2.1 global climate model, but uses atmosphere and ocean components with much finer horizontal resolution. The goals are at least twofold: (a) to be able to more faithfully model the effects of smaller-scale processes in the climate system, and (b) to better simulate climate and its change on regional spatial scales. A specific focus has been the development and incorporation of an ocean component that is far more energetic and realistic than the ocean component of the GFDL CM2.1 model. The strategy to achieve this goal included the use of significantly finer horizontal resolution, a higher order advection scheme, very low viscosity, and the absence of explicit lateral diffusion.

We present the results from two main simulations with CM2.5, a 280-year control simulation and a 140-year idealized climate change simulation. Analysis of the control simulation shows marked improvement in the simulation of many aspects of climate, including on regional scales, relative to the coarser resolution CM2.1 model. The simulation of the tropics is notably improved, with substantially reduced biases, and an improved simulation of ENSO. Biases in SST off the west coast of South America and the southwestern coast of North America were virtually eliminated. The simulation of the Indian monsoon is substantially improved, as is precipitation simulation over many continental regions, including South America, North America, and Europe. As measured by the Koppen climate classification system, the error in the simulation of continental climate is reduced by 26% in CM2.5 versus CM2.1. The improved representation of orography, both in the atmosphere and ocean, is clearly one important factor in the improved simulation characteristics. Results also point to the importance of explicitly resolving smaller scale processes, such as oceanic mesoscale eddies, although additional studies are necessary to more thoroughly assess this.

Climate change simulations show many similarities with results using the lower resolution CM2.1 model, but some intriguing differences emerge. Two of the most significant differences in response to doubled CO_2 are enhanced warming of the near-surface in the Southern Ocean in CM2.5 relative to CM2.1, and a change in the precipitation response over the Mediterranean region. In CM2.5 the reduction in precipitation in response to CO_2 is largely associated with topographic features, whereas the precipitation reduction in CM2.1 is more broad-scale in character. The CM2.1 results are largely consistent with the ensemble of models assessed in the IPCC AR4.

The primary goals of this paper are to document and describe the CM2.5 model, and to highlight those aspects of the simulations of the control climate and the climate change simulations that are different in CM2.5 versus CM2.1. Detailed analyses of the reasons for these differences will be the subject of future investigations.

Acknowledgements

The authors would like to thank Bruce Wyman, Isaac Held, SJ Lin, and Ming Zhao for assistance with the implementation of their high-resolution atmosphere model within the framework of the coupled model CM2.5, and Kirsten Findell and Mike Winton for very helpful comments on an earlier version of the manuscript. The authors would also like to thank Amy Langenhorst for help with the FRE software package, and Frank Indiviglio for assistance in facilitating the execution priority of the CM2.6 model. The authors wish to acknowledge use of the Ferret program for analysis and graphics in this paper. Ferret is a product of NOAA's Pacific Marine Environmental Laboratory. (Information is available at http://ferret.pmel.noaa.gov/Ferret/)

References

Adler, R.F., G.J. Huffman, A. Chang, R. Ferraro, P. Xie, J. Janowiak, B. Rudolf, U. Schneider, S. Curtis, D. Bolvin, A. Gruber, J. Susskind, and P. Arkin, 2003: The Version 2 Global Precipitation Climatology Project (GPCP) Monthly Precipitation Analysis (1979-Present). *J. Hydrometeor.*, **4**,1147-1167.

An, S.-I., and B. Wang, 2000: Interdecadal change of the structure of the ENSO mode and its impact on the ENSO frequency. *J. Climate*, **13**, 2044-2055.

Annamalai, H., K. Hamilton, and K. R. Sperber, 2007: South Asian summer monsoon and its relationship with ENSO in the IPCC-AR4 simulations. *J. Climate*, **20**, 1071–1092

Antonov, J. I., S. Levitus, T. P. Boyer, M. E. Conkright, T. D. O'Brien, and C. Stephens, 1998: World Ocean Atlas 1998 Vol. 1: Temperature of the Atlantic Ocean, NOAA Atlas NESDIS 27, U.S. Government Printing Office, Washington, D.C.

Böning, C. W., M. Scheinert, J. Dengg, A. Biastoch, and A. Funk (2006), Decadal variability of subpolar gyre transport and its reverberation in the North Atlantic overturning, *Geophys. Res. Lett.*, **33**, L21S01, doi:10.1029/2006GL026906.

Boyer, T. P., S. Levitus, J. I. Antonov, M. E. Conkright, T. D. O'Brien, and C. Stephens, 1998: World Ocean Atlas 1998 Vol. 4: Salinity of the Atlantic Ocean, NOAA Atlas NESDIS 30, U.S. Government Printing Office, Washington, D.C.

Capotondi, A., A. Wittenberg, and S. Masina, 2006: Spatial and temporal structure of tropical Pacific interannual variability in 20th century coupled simulations. *Ocean Modelling*, **15**, 274-298.

Collins M., 2005: El Niño- or La Niña-like climate change?. *Clim. Dyn.*, **24**(1), 89-104.

Collins, M., S.-I. An, W. Cai, A. Ganachaud, E. Guilyardi, F.-F. Jin, M. Jochum, M. Lengaigne, S. Power, A. Timmermann, G. Vecchi, and A. Wittenberg, 2010: The impact of global warming on the tropical Pacific and El Niño. *Nature Geoscience*, **3**, 391-397. doi:10.1038/ngeo868

Cunningham, S. A., S. G. Alderson, B. A. King, and M. A. Brandon, 2003: Transport and variability of the Antarctic Circumpolar Current in Drake Passage. J. Geophys. Res., 108, 8084,doi:10.1029/2001JC001147.

Danabasoglu, G., W. G. Large, and B. P. Briegleb (2010), Climate impacts of parameterized Nordic Sea overflows, *J. Geophys. Res.*, 115, C11005, doi:10.1029/2010JC006243.

DiNezio, P, A. Clement, and G.A. Vecchi (2010): Reconciling Differing Views of Tropical Pacific Climate Change. *EOS, Trans. Amer. Geophys. Union*, **91**(16), 141-152.

Flato, G. M., and G. J. Boer (2001), Warming asymmetry in climate change simulations, *Geophys. Res. Lett.*, 28(1), 195–198, doi:10.1029/2000GL012121

Fox-Kemper, B., G. Danabasoglu, S.M. Griffies, R.W. Hallberg, M.M. Holland, S. Peacock, and B. Samuels, 2010, Parameterization of mixed-layer eddies. III: Implementation and impact in global ocean climate simulations**.** *Ocean Modelling*. doi:10.1016/j.ocemod.2010.09.002. 9/10.

Gent, P.R., S. G. Yeager, R.B. Neale, S. Levis, and D.A. Bailey, 2010: Improvements in a half degree atmosphere/land version of the CCSM. *Clim. Dynamics*, 34, 6, 819-833, doi: 10.1007/s00382-009-0614-8.

GFDL Global Atmospheric Model Development Team, 2004: The new GFDL global atmosphere and land model AM2/LM2: Evaluation with prescribed SST simulations. *J. Climate*, **17**, 4641-4673.

Gnanadesikan, A, and coauthors, 2006**:** GFDL's CM2 Global Coupled Climate Models. Part II: The baseline ocean simulation**.** *Journal of Climate*, **19(5)**, doi:10.1175/JCLI3630.1.

Gnanadesikan, A., and R. J Stouffer, 2006: Diagnosing atmosphere-ocean general circulation model errors relevant to the terrestrial biosphere using the Köppen climate classification. *Geophysical Research Letters*, **33**, L22701, doi:10.1029/2006GL028098.

Griffies, S.M., 2010, ELEMENTS OF MOM4P1, GFDL OCEAN GROUP TECHNICAL REPORT NO. 6, NOAA/Geophysical Fluid Dynamics Laboratory, 444 pages, Version prepared on February 19, 2010, Code and documentation available online at www.gfdl.noaa.gov/fms.

Griffies, S.M., and R.W. Hallberg, 2000**:** Biharmonic friction with a Smagorinsky-like viscosity for use in large-scale eddy-permitting ocean models**.** *Monthly Weather Review*, 128(8)**,** 2935-2946.

Griffies, S.M., et al., 2005**:** Formulation of an ocean model for global climate simulations**.** *Ocean Science*, **1**, 45-79.

Griffies, S.M. et al., 2009: Coordinated ocean-ice reference experiments (COREs). *Ocean Modelling*, 26(1-2), doi:10.1016/j.ocemod.2008.08.007.

Griffies, S.M., et al, 2011: GFDL's CM3 Coupled climate model: characteristics of the ocean and sea ice simulations. *Journal of Climate accepted*.

Guilyardi, E., A. Wittenberg, A. Fedorov, M. Collins, C. Wang, A. Capotondi, G. J. van Oldenborgh, and T. Stockdale, 2009: Understanding El Niño in ocean-atmosphere general circulation models: Progress and challenges. *Bull. Amer. Meteor. Soc.*, **90**, 325-340. doi:10.1175/2008BAMS2387.1

Hallberg, R. and A. Gnanadesikan, 2006: The role of eddies in determining the structure and response of the wind-driven Southern Hemisphere overturning: Results from the Modeling Eddies in the Southern Ocean (MESO) project. J. Phys. Oceanogr., 36, 2232–2252.

Held, I. M., and B. J. Soden, 2006: Robust responses of the hydrological cycle to global warming. *J. Climate*, **19**, 5686–5699.

Held, I., T.L. Delworth, J. Lu, K. Findell, and T.R. Knutson, 2005: Simulation of Sahel drought in the 20th and 21st centuries. *Proceedings of the National Academy of Sciences*, **102**(50), doi:10.1073/pnas.0509057102.

Hunke, E.C., and J.K. Dukowicz, 1997: An elastic-viscous-plastic model for sea ice dynamics, *J. Phys. Oceanogr.*, **27**, 1849—1867.

Huynh, H.T., 1996: Schemes and constraints for advection, in: Proceedings of the Fifteenth International Conference on Numerical Methods in Fluid Dynamics, Monterey, CA, USA, 24–28 June 1996.

Johns, W. E., M. O. Baringer, L. M. Beal, S. A. Cunningham, T. Kanzow, H. L. Bryden, J. 1496 Hirschi, J. Marotzke, C. Meinen, B. Shaw, and R. Curry, 2011. Continuous, array-based 1497 estimates of Atlantic Ocean heat transport at 26.5 ºN. *J. Clim*., in press.

Kanzow. T., S.A. Cunningham, W.E. Johns, J. J-M. Hirschi, J. Marotzke, M. O. Baringer, C.S. 1502 Meinen, M. P. Chidichimo, C. Atkinson, L. M. Beal, H. L. Bryden, J. Collins, 2010. 1503 Seasonal variability of the Atlantic meridional overturning circulation at 26.5_{o}N. *Journal of* 1504 *Climate*, *23*, doi: 10.1175/2010JCLI3389.1171.

Kim, D., J.-S. Kug, I.-S. Kang, F.-F. Jin, and A. T. Wittenberg, 2008: Tropical Pacific impacts of convective momentum transport in the SNU coupled GCM. *Climate Dyn.*, **31**, 213-226. doi:10.1007/s00382-007-0348-4.

Kirtman, B. P., 1997: Oceanic Rossby wave dynamics and the ENSO period in a coupled model. *J. Climate*, **10**, 1690-1704.

Kistler, R., and Coauthors, 2001: The NCEP-NCAR 50-year reanalysis: Monthly means CD-ROM and documentation. *Bull. Amer. Meteor. Soc.*, **82**, 247-268.

Kottek, M., J. Grieser, C. Beck, B. Rudolf, and F. Rubel, 2006: World map of the Koppen climate classification updated. *Meteorologische Zeitschrift*, **15**I3), 259-263.

Kug, J.-S., J. Choi, S.-I. An, F.-F. Jin, and A. T. Wittenberg, 2010: Warm pool and cold tongue El Niño events as simulated by the GFDL CM2.1 coupled GCM. *J. Climate*, **23**, 1226-1239. doi:10.1175/2009JCLI43293.1

Large, W.G, J.C. McWilliams, and S.C. Doney, 1994: Oceanic vertical mixing: A review and a model with a nonlocal boundary layer parameterization. *Reviews of Geophysics*. **32,** 363-403.

Larkin, N. K., and D. E. Harrison, 2005: On the definition of El Niño and associated seasonal average U.S. weather anomalies, *Geophys. Res. Lett.*, **32**, L13705, doi:10.1029/2005GL022738.

Le Traon, P.-Y., F. Nadal, and N. Ducet, 1998: An improved mapping method of multisatellite altimeter data. *J. Atmos. Oceanic Technol.*, **15**, 522-534 (1998).

Lee, H. C., A. Rosati, and M. J. Spelman, 2006: Barotropic tidal mixing effects in a coupled climate model: Oceanic conditions in the North Atlantic. *Ocean Modell.*, **11**, 467-477

Lee, H.-C., T.L. Delworth, A. Rosati, R. Zhang, W. Anderson, F. Zeng, C. Stock, and A. Gnanadesikan, K. Dixon, S.M. Griffies,2011: Impact of climate warming on upper layer of the Bering Sea. In preparation.

Legates, D. R. and C. J. Willmott(1990b) Mean Seasonal and Spatial Variability in Gauge-Corrected, Global Precipitation. *International Journal of Climatology*, **10**, 111-127.

Lin, S-J., 2004: A "vertically Lagrangian" finite-volume dynamical core for global models. *Monthly Weather Review*, **132(**10), 2293-2307.

Manabe, S., R.J. Stouffer, M.J. Spelman, and K. Bruan, 1991: Transient responses of a coupled ocean-atmosphere model to gradual changes of atmospheric CO_2. Part I: Annual mean response**.** *Journal of Climate*, **4**(8), 785-818.

Martin, T, and Alistair Adcroft, July 2010**:** Parameterizing the fresh-water flux from land ice to ocean with interactive icebergs in a coupled climate model. *Ocean Modelling*, **34**(3-4), doi:10.1016/j.ocemod.2010.05.001.

Meehl, G.A., T.F. Stocker, W.D. Collins, P. Friedlingstein, A.T. Gaye, J.M. Gregory, A. Kitoh, R. Knutti, J.M. Murphy, A. Noda, S.C.B. Raper, I.G. Watterson, A.J. Weaver and Z.-C. Zhao, 2007: Global Climate Projections. In: *Climate Change 2007: The Physical Science Basis. Contribution of Working Group I to the Fourth Assessment Report of the Intergovernmental*

Panel on Climate Change [Solomon, S., D. Qin, M. Manning, Z. Chen, M. Marquis, K.B. Averyt, M. Tignor and H.L. Miller (eds.)]. Cambridge University Press, Cambridge, United Kingdom and New York, NY, USA.

Milly, P.C., and A B Shmakin, 2002: Global modeling of land water and energy balances. Part I: The land dynamics (LaD) model. *Journal of Hydrometeorology*, **3(3)**, 283-299.

Murray, R.J., 1996: Explicit generation of orthogonal grids for ocean models. *Journal of Computational Physics*, **126**, 251-273.

Pacanowski, R.C., 1987: Effect of equatorial currents on surface stress. *Journal of Physical Oceanography,* 17, 833-838.

Perovich, D., T.C. Grenfell, B. Light, and P.V. Hobbs, 2002: Seasonal evolution of the albedo of multiyear Arctic sea ice. *Journal of Geophysical Research*, **107(C10)**, 8044, doi:10.1029/2000JC000438,

Putman, W M., and Shian-Jiann Lin, 2007: Finite-volume transport on various cubed-sphere grids**.** *Journal of Computational Physics*, **227**(1), 55-78.

Rajeevan, M. and Nanjundiah RS, 2009: Coupled model simulations of twentieth century climate of the Indian summer monsoon, Current Trends in Science, N. Mukunda (ed), Platinum Jubilee Publication of Indian Academy of Sciences, Bangalore, India, 537-568. (available at http://www.ias.ac.in)

Sakamato, T.T., and coauthors, MIROC4h - a new high resolution atmosphere-ocean coupled general circulation model. Submitted to the Journal of the Meteorological Society of Japan.

Shaffrey, L. C., and Coauthors, 2009: U.K. HiGEM: The New U.K. High-Resolution Global Environment Model—Model Description and Basic Evaluation. *J. Climate*, **22**, 1861–1896. doi: 10.1175/2008JCLI2508.1

Simmons, A. J., and J. K. Gibson, 2000: The ERA-40 project plan. Tech. Rep., ERA-40 Project Report Series 1, ECMWF, Reading, United Kingdom, 63 pp.

Simmons, H.L., S.R. Jayne, L.C. St. Laurent, and A.J. Weaver, 2004: Tidally driven mixing in a numerical model of the ocean general circulation. *Ocean Modelling*, **6,** 245-263**.**

Smith, T. M., R. W. Reynolds, T. C. Peterson, and J. Lawrimore, 2008: Improvements to NOAA's historical merged land-ocean surface temperature analysis (1880-2006), *J. Climate*, **21**, 2283-2296.

Steele, M., R. Morfley, and W. Ermold, 2001: PHC: A global ocean hydrography with a high-quality Arctic Ocean, *J. Climate*, **14**, 2079-2087.

Vecchi, G. A., and A. T. Wittenberg, 2010: El Niño and our future climate: Where do we stand? *Wiley Interdisciplinary Reviews: Climate Change*, **1**, 260-270. doi:10.1002/wcc.33

Vecchi, G.A., and B.J. Soden (2007). Global Warming and the Weakening of the Tropical Circulation. *J. Climate*, **20**(17), 4316-4340.

White, L., and A. Adcroft, 2008: A high-order finite volume remapping scheme for nonuniform grids: the piecewise quartic method (PQM), *J. Comput. Phys.,* **227**, 7394–7422.

Winton, M., 2000: A reformulated three-layer sea ice model. *J. Atmos. Ocean. Tech.*, **17**, 525—531.

Winton, M., R.W. Hallberg, and A. Gnanadesikan, 1998**:** Simulation of density-driven frictional downslope flow in z-coordinate ocean models. *Journal of Physical Oceanography*, **28(11)**, 2163-2174.

Winton, M., 2000: A reformulated three-layer sea ice model. *J. Atmos. Ocean. Tech.*, **17**, 525—531.

Wittenberg, A. T., 2002: ENSO response to altered climates. Ph.D. thesis, Princeton University. 475pp.

Wittenberg, A. T., 2009: Are historical records sufficient to constrain ENSO simulations? *Geophys. Res. Lett.*, **36**, L12702. doi:10.1029/2009GL038710.

Wittenberg, A. T., A. Rosati, N.-C. Lau, and J. J. Ploshay, 2006: GFDL's CM2 global coupled climate models, Part III: Tropical Pacific climate and ENSO. *J. Climate*, **19**, 698-722.

Xie P., and P. A. Arkin, 1997: Global precipitation: a 17-year monthly analysis based on gauge observations, satellite estimates, and numerical model outputs. Bull. Amer. Meteor. Soc., 78, 2539-2558.

Zhang, R., T.L. Delworth, A. Rosati, W.G. Anderson, K.W. Dixon, H.-C. Lee, and F. Zeng,: Sensitivity of the North Atlantic Ocean Circulation to an Abrupt Change in the Nordic Sea Overflow in a High Resolution Global Coupled Climate Model. *Submitted to Journal of Geophysical Research-Oceans.*

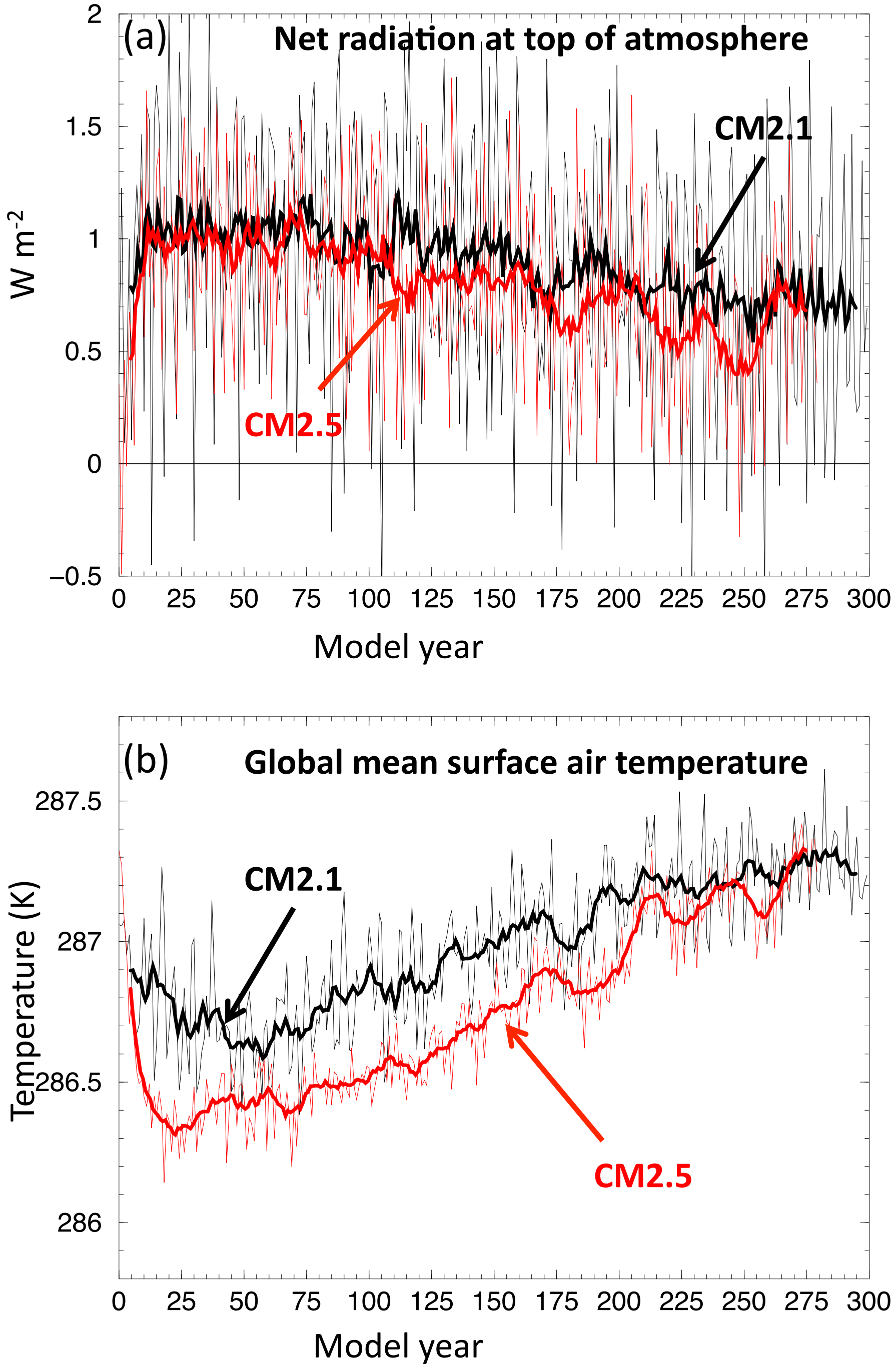

Figure 1 Model results from 1990 control simulations using CM2.1 and CM2.5. (a) Time series of global mean, annual mean net radiation at the top of the atmosphere. Units are W m^{-2}. Thin black (red) lines are yearly values for CM2.1 (CM2.5), while thick black (red) lines are smoothed with a 10 year running mean. (b) Same as (a), but for near-surface air temperature.

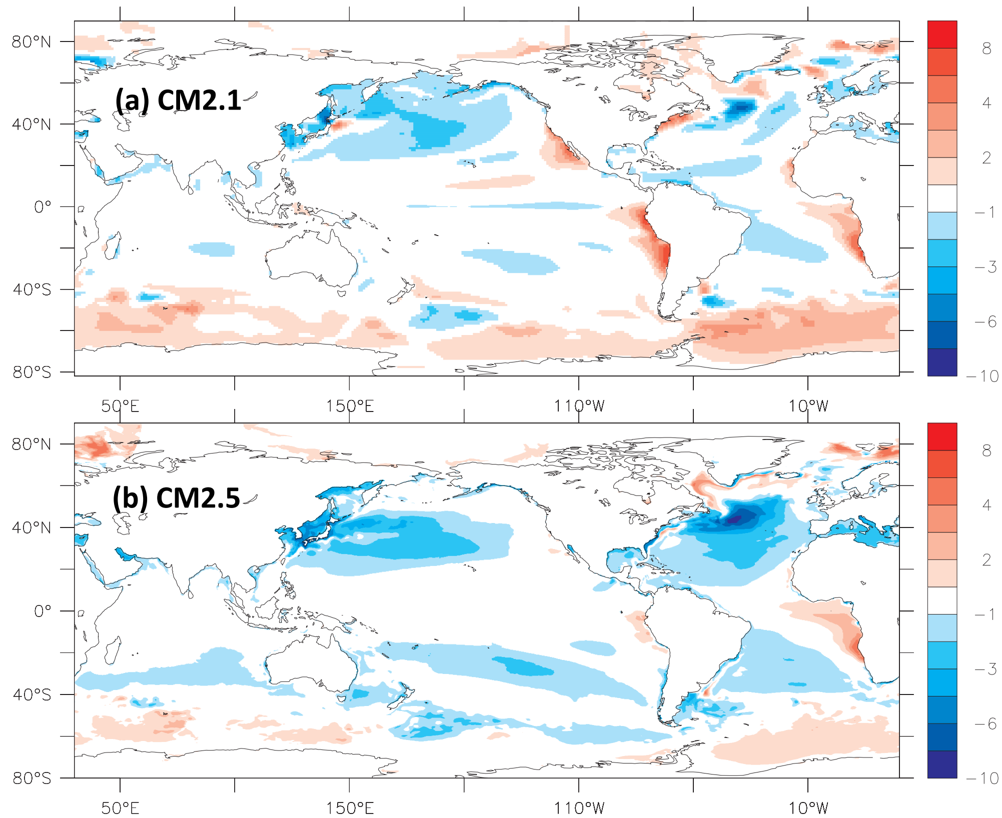

Figure 2 Maps of errors in simulation of annual mean sea-surface temperature (SST). Units are K. The errors are computed as model minus observations, where the observations are from the Reynolds SST data (provided by the NOAA-CIRES Climate Diagnostics Center, Boulder, Colorado, USA, from their Web site at http://www.cdc.noaa.gov/). For the models, the annual mean, time-mean over years 101-200 of the 1990 Control simulations are used. Contour interval is 1K, except that there is no shading for values between –1 K and +1 K. Positive values indicate the model is warmer than observations. (a) CM2.1. (b) CM2.5.

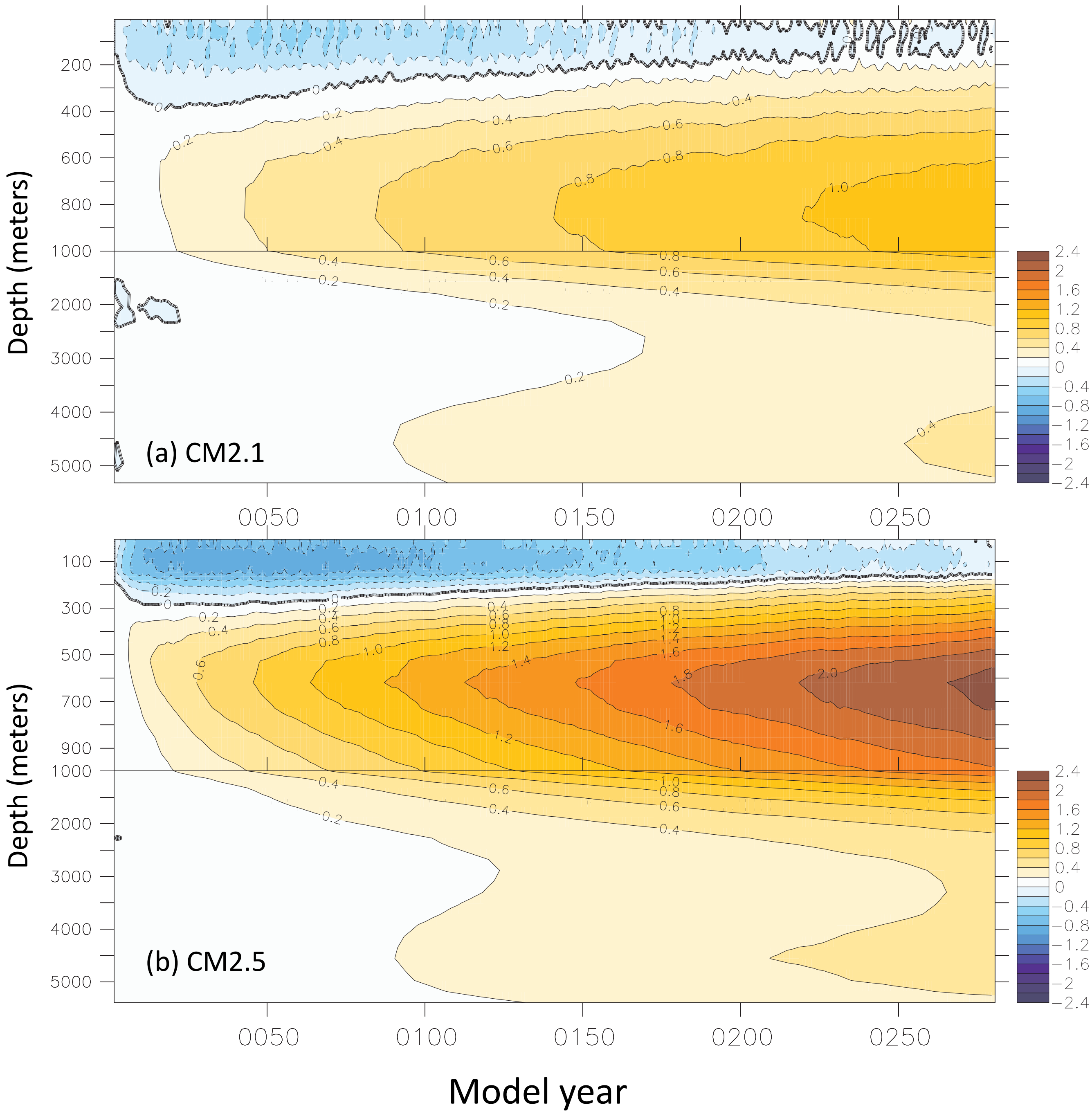

Figure 3 Subsurface ocean temperature drift from initial conditions. The values plotted are the differences between the global mean, annual mean temperature at each year minus the global mean, annual mean value at year 1. Units are K. Positive (negative) values indicate the subsurface ocean has warmed (cooled). Note the difference in the vertical scales above and below 1000 m. (a) CM2.1. (b) CM2.5.

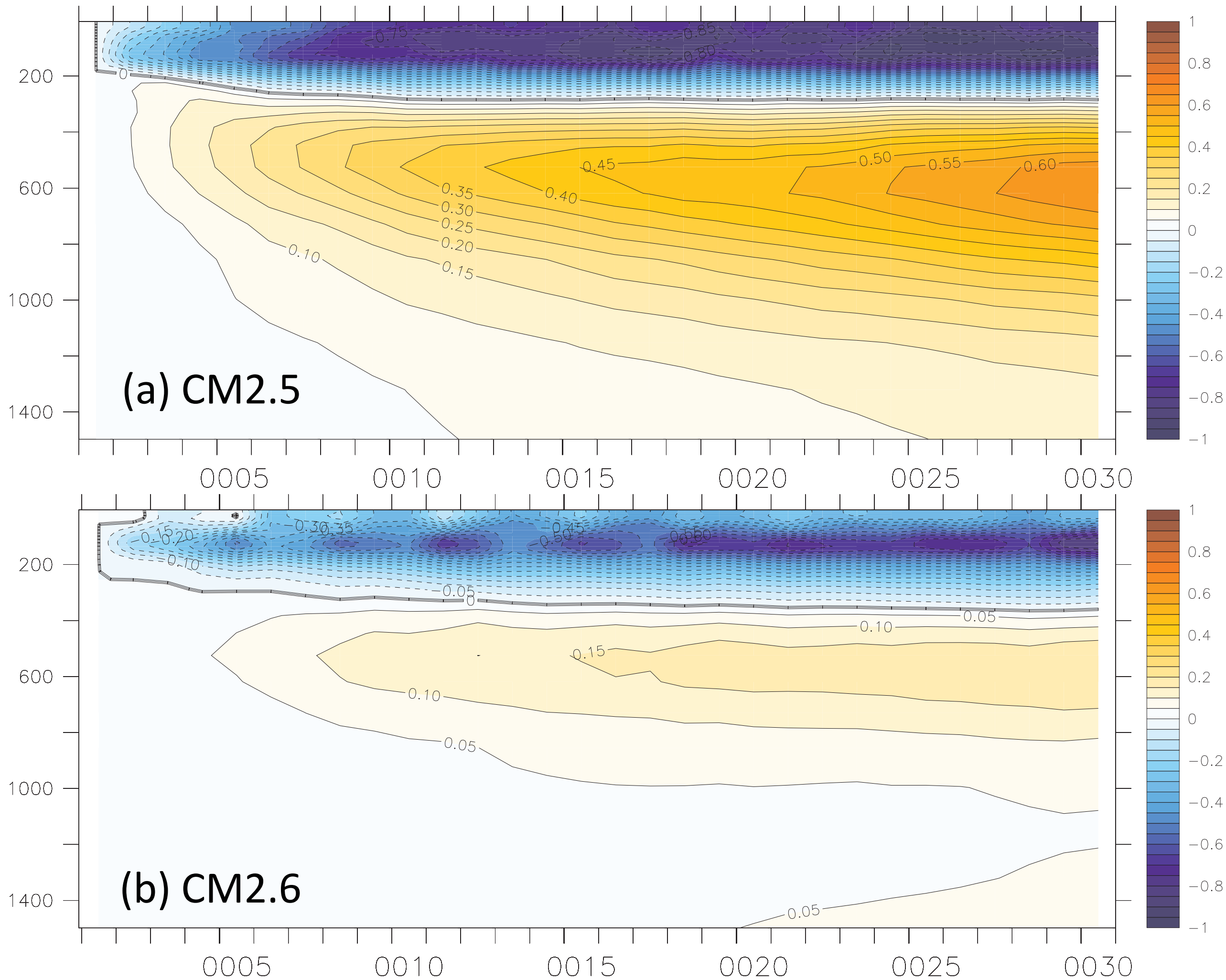

Figure 4 Subsurface ocean temperature drift from initial conditions. The values plotted are the differences between the global mean, annual mean temperature at each year minus the annual mean value at year 1. Positive (negative) values indicate the subsurface ocean has warmed (cooled). Units are K. (a) CM2.5 (b) CM2.6

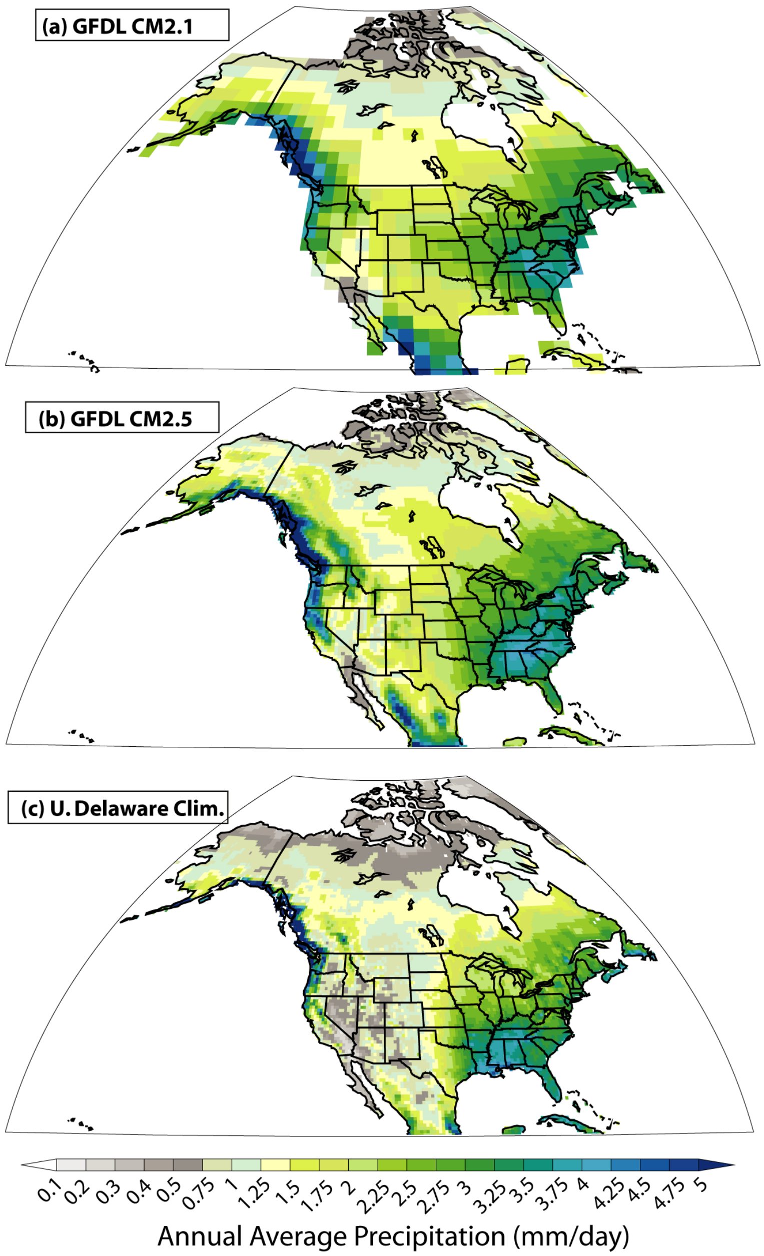

Figure 5 Annual mean precipitation over land areas, units are mm day^{-1}. For model output, annual means from years 101-200 of the 1990 Control simulations are used. (a) CM2.1. (b) CM2.5 (c) Observed, data from University of Delaware (Legates and Wilmott, 1990; updated data available at http://climate.geog.udel.edu/~climate/html_pages/precip_clim.html). Note the non-linear contour scale.

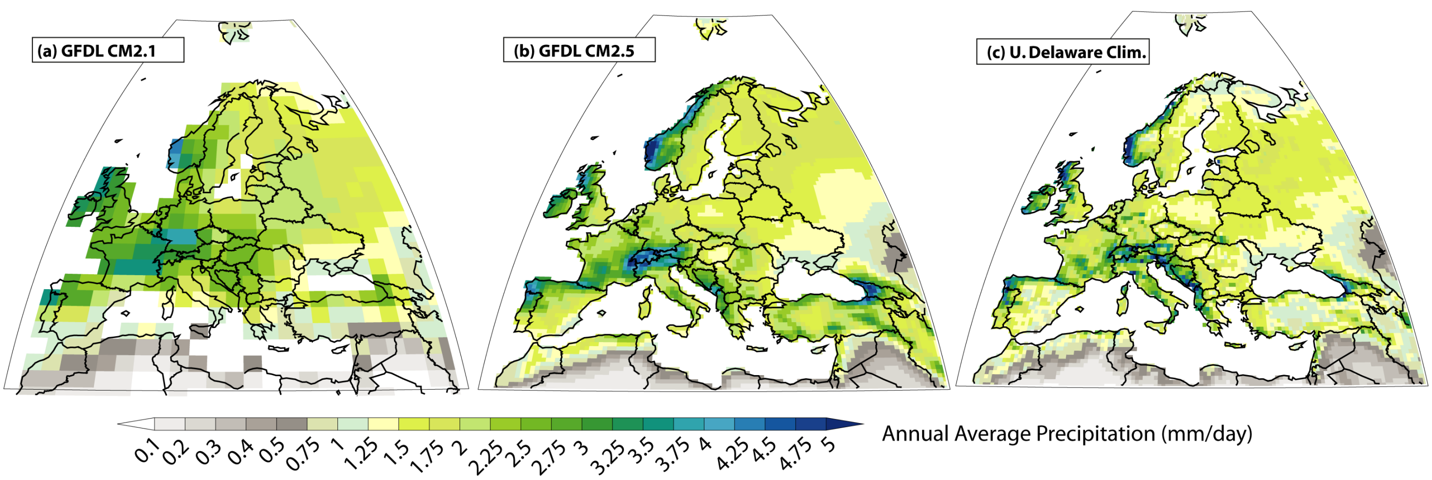

Figure 6 Annual mean precipitation, units are mm day^{-1}. For model output, time-mean, annual mean data from years 101-200 of the 1990 Control simulations is used. (a) CM2.1 (b) CM2.5 (c) Observed (Legates and Wilmott, 1990).

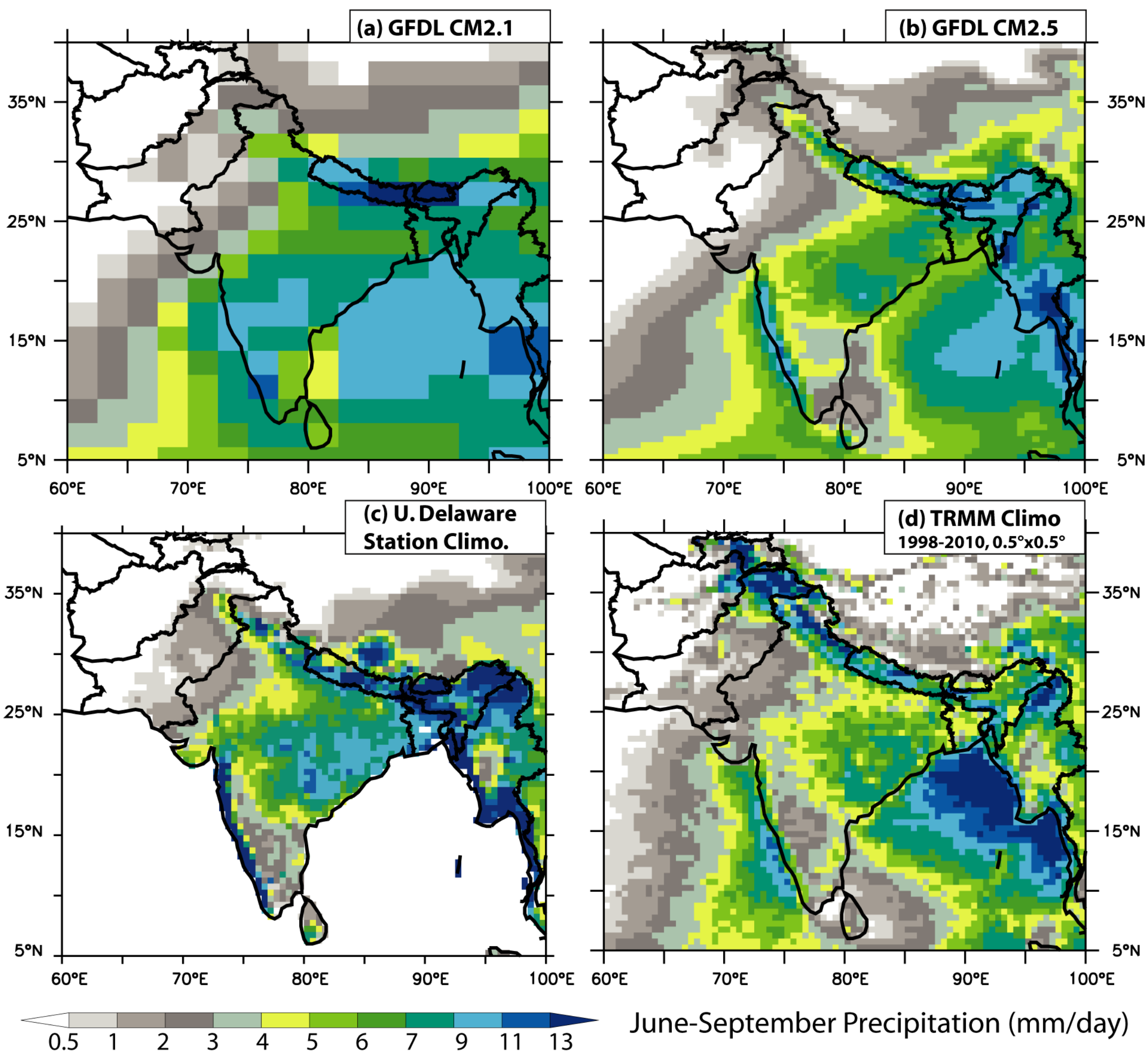

Figure 7 Precipitation averaged over the months of June-September, units are mm day^{-1}. For model output, time-mean data from years 101-200 of the 1990 Control simulations are used. (a) CM2.1 (b) CM2.5 (c) Observed data over land areas from U. Delaware (Legates and Wilmott, 1990. (d) Observed, data from TRMM satellite mission (TRMM-PR Product "3A12: Monthly 0.5 x 0.5 degree mean 2A12, profile, and surface rainfall", downloaded from the NASA-MIRADOR data server: http://mirador.gsfc.nasa.gov/)

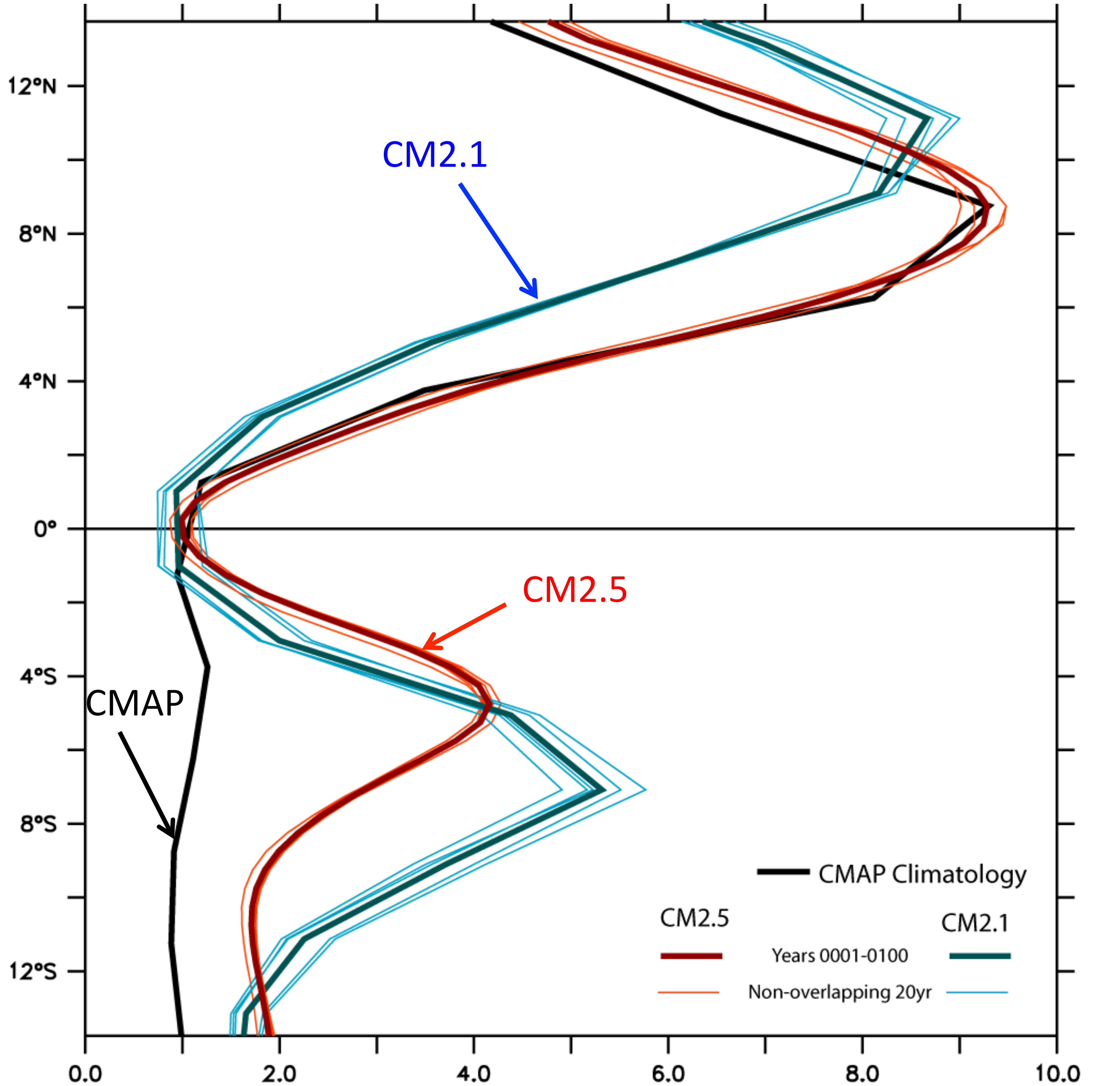

Figure 8 Annual mean precipitation, units are mm day^{-1}. The thin red and blue lines show the distribution of the five separate 20-year mean precipitation values over the period of years 101-200, while the thick red and blue lines show the 100-year mean values. The clustering of the 20-year means around the 100-year means suggests the differences between CM2.1 and CM2.5 are robust. The CMAP data are described in Adler et al. (2003), and the GPCP data are described in Xie et al. (1997).

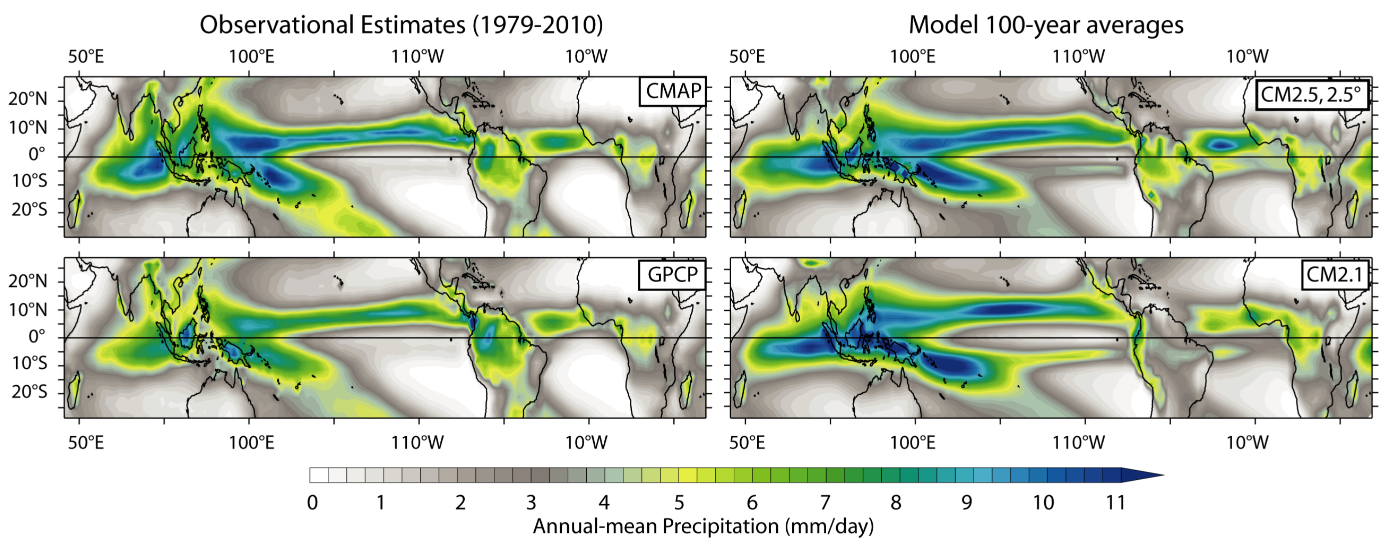

Figure 9 Annual mean precipitation, units are mm day^{-1}. Left column shows observational estimates, right column shows simulated precipitation. Note that the CM2.5 results are plotted on a grid that is much coarser than its native model grid, but on a grid similar to CM2.1 and the observations.

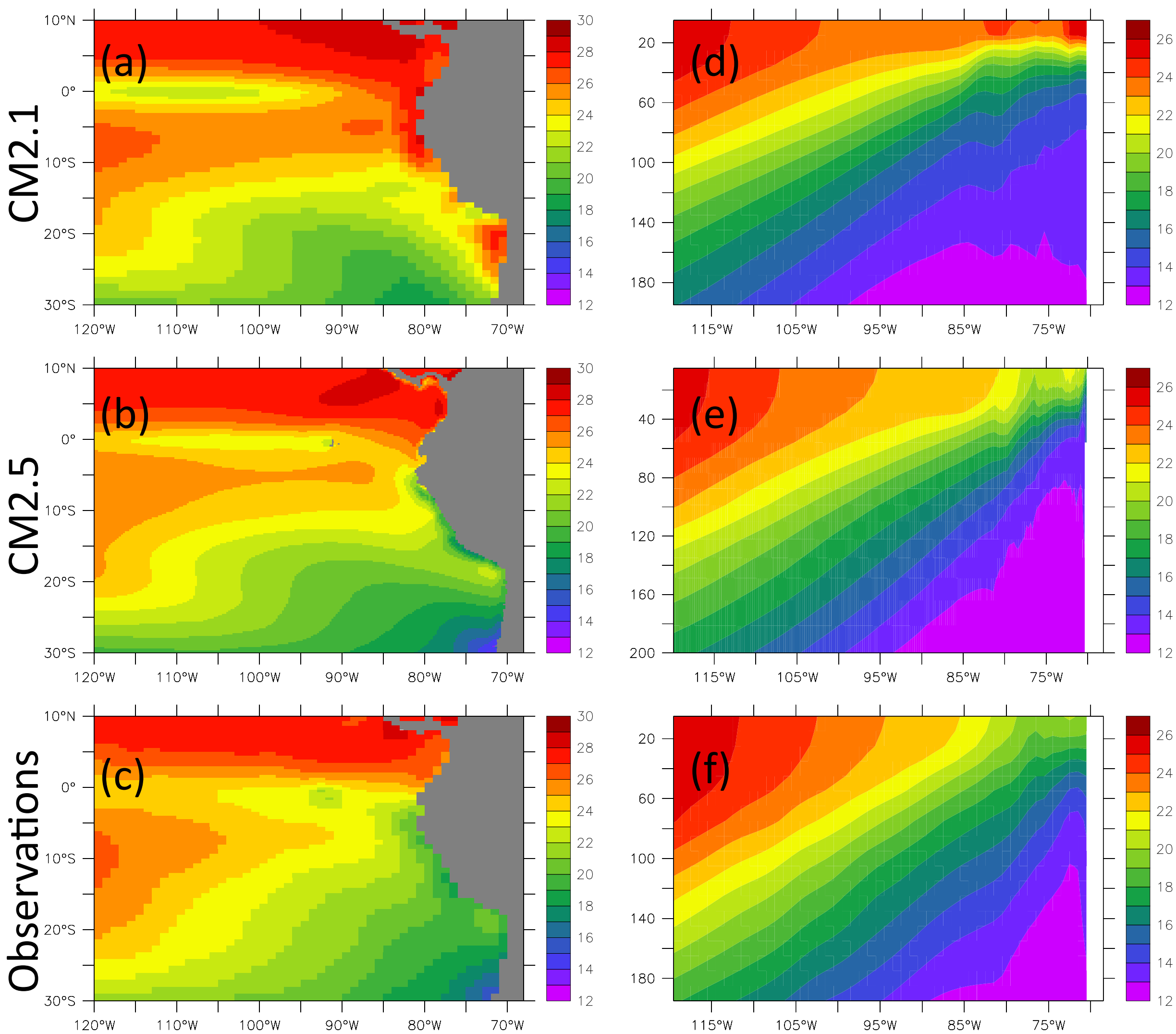

Figure 10 (a) Sea Surface Temperature (SST) from CM2.1 Control, calculated as annual mean over years 101-200. Units are ^{o}C. (b) Same as (a), for CM2.5. (c) Observed SST (Antonov et al., 1998). (d) Cross-section of annual mean temperature averaged over years 101-200, and averaged over latitudes 5^{o}S-20^{o}S. Data from CM2.1 Control. (e) Same as (d) , but from CM2.5 Control. (f) Same as (d), but data from observations (Antonov et al., 1998).

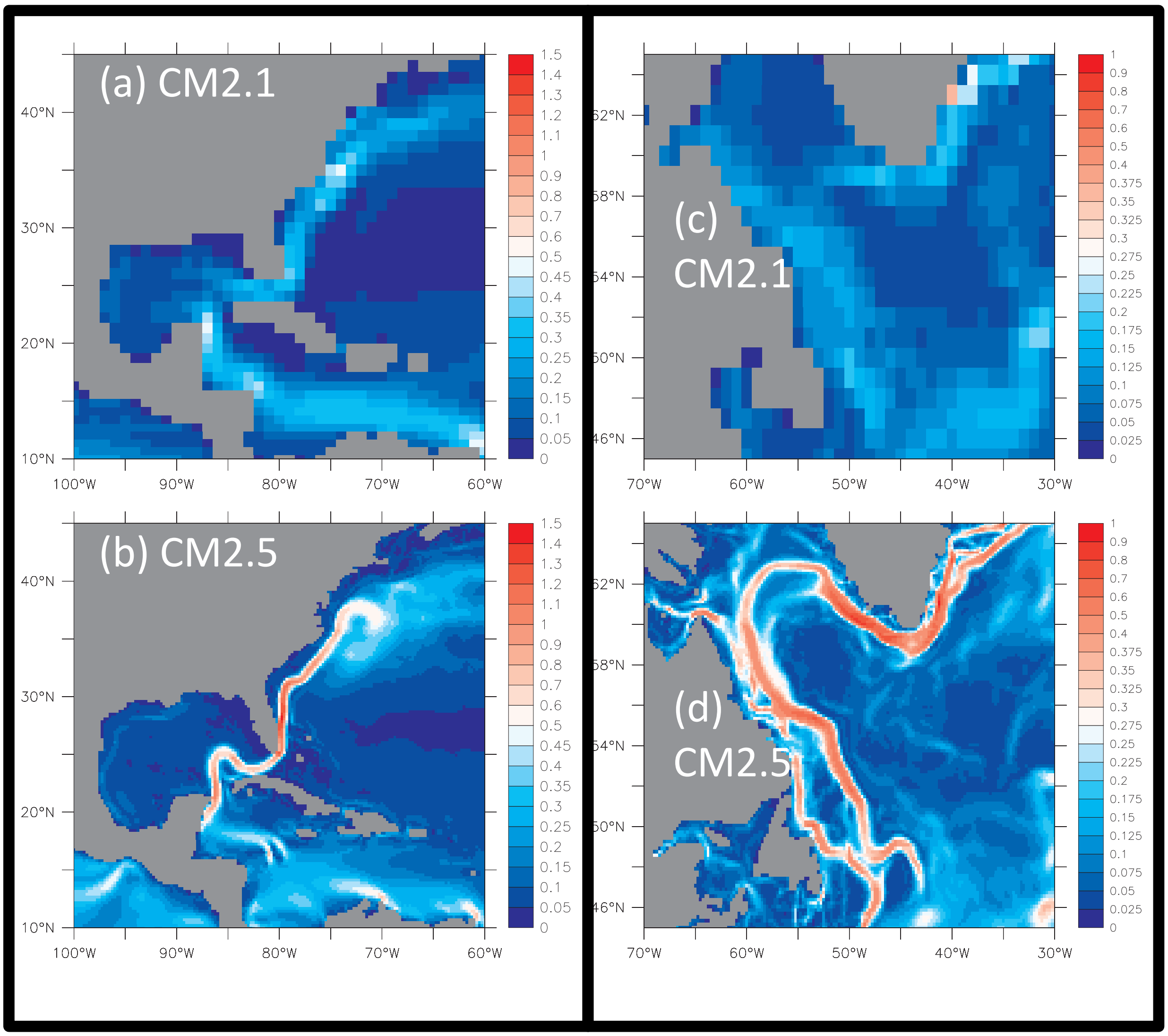

Figure 11 Annual mean surface current speed, units are m s^{-1}. Gulf Stream region for (a) CM2.1 and (b) CM2.5. Labrador Sea region for (c) CM2.1 and (d) CM2.5. All values plotted are annual mean averages over the period of years 101-200 of the 1990 control runs.

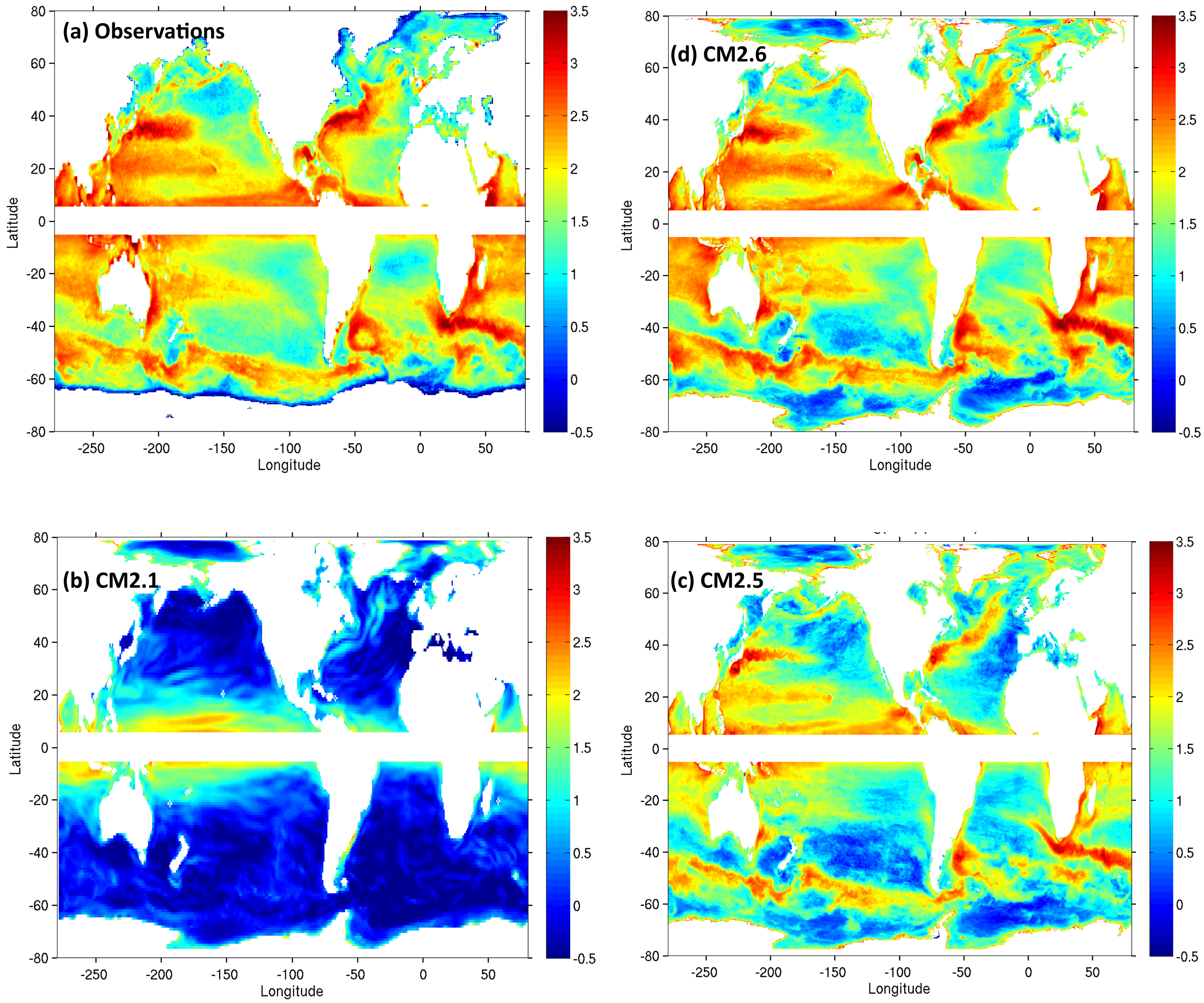

Figure 12 Maps of the logarithm of Eddy Kinetic Energy (EKE); units are $cm^2 s^{-2}$. In these calculations we start from sea surface height – available directly from the model simulations, and from satellite altimetry in the observations (LeTraon et al, 1998). We use instantaneous values taken every 7 days. The period 2002-2006 is used for the observations, and years 6-10 for the models. The sea surface heights are used to compute near-surface currents using geostrophy. Eddy velocities are computed as deviations from the long-term mean, from which EKE is then calculated and plotted on a logarithmic scale. No values are plotted within 5 degree of the Equator, since the geostrophic approximation is not fully valid there. (a) Observations, (b) CM2.1, (c) CM2.5, (d) CM2.6

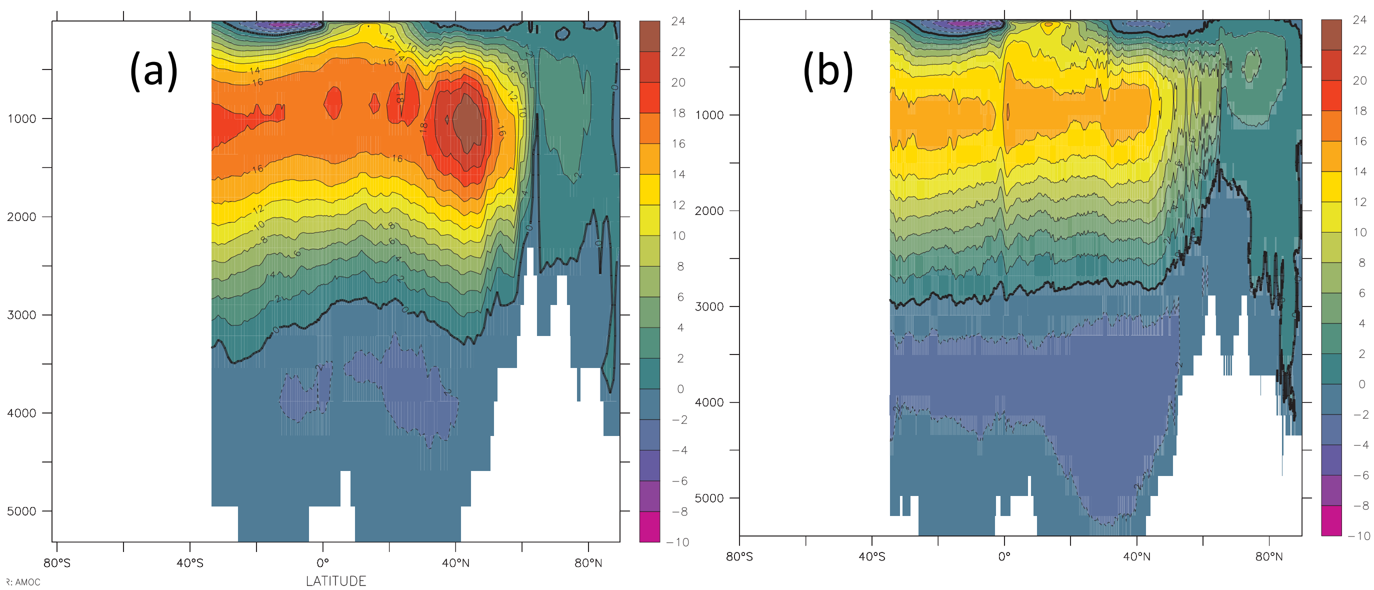

Figure 13 (a) Spatial pattern of the Atlantic Meridional Overturning Circulation (AMOC) in CM2.1. This field is computed as the definite integral of the meridional volume transport across the North Atlantic, and the indefinite integral from the ocean bottom to the surface. Units are Sverdrups (10^6 m^3 s^{-1}). Flow is clockwise around a maximum value in the depth-latitude plane in the figure above. Calculations are done using annual-mean, time-mean data for years 101-200 of the 1990 Control simulation. (b) Same as (a), but for CM2.5.

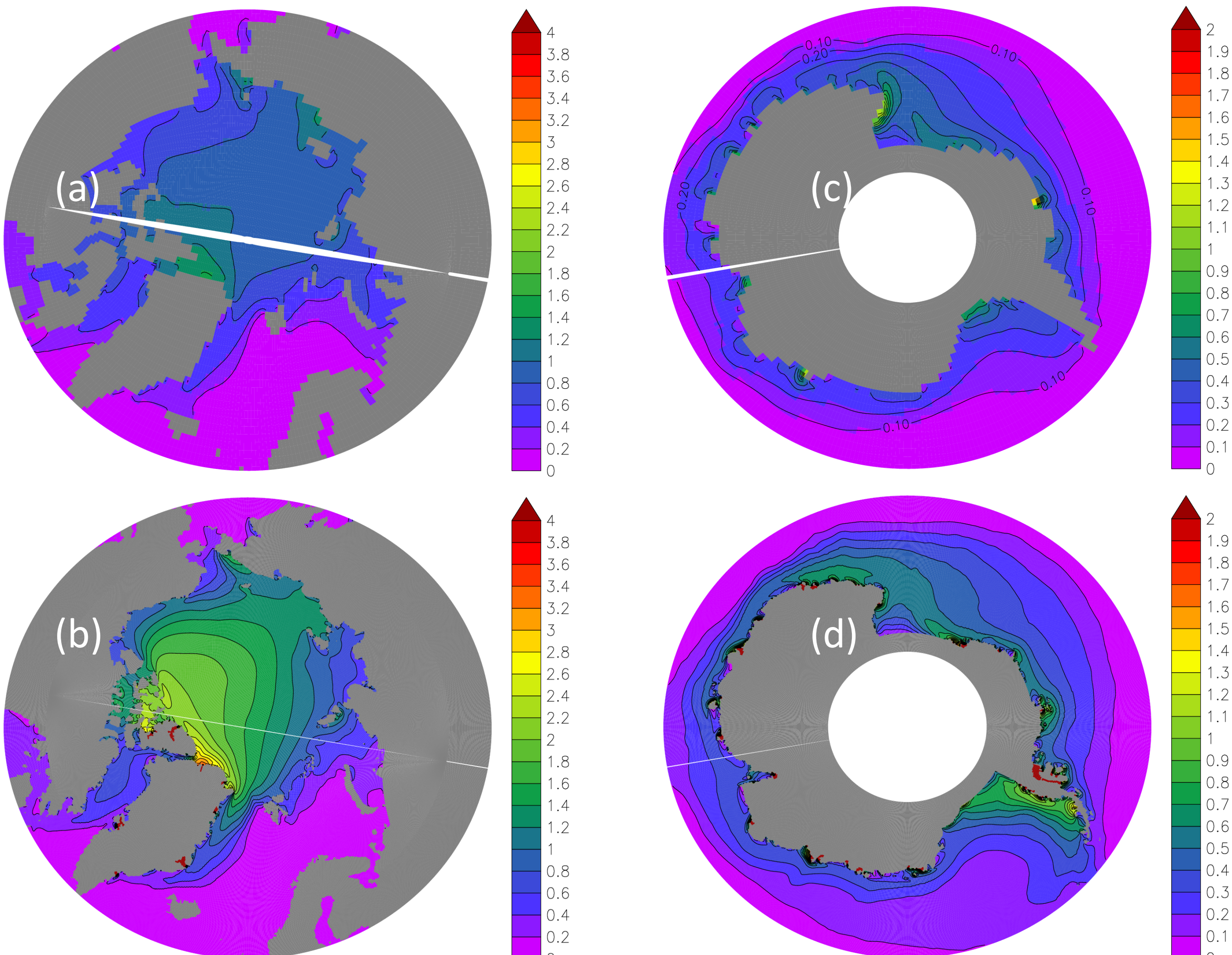

Figure 14 Annual mean sea ice thickness (meters). (a) CM2.1, Northern Hemisphere, (b) CM2.5, Northern Hemisphere, (c) CM2.1, Southern Hemisphere, (d) CM2.5, Southern Hemisphere. Note that there are different shading levels for the Northern and Southern Hemispheres.

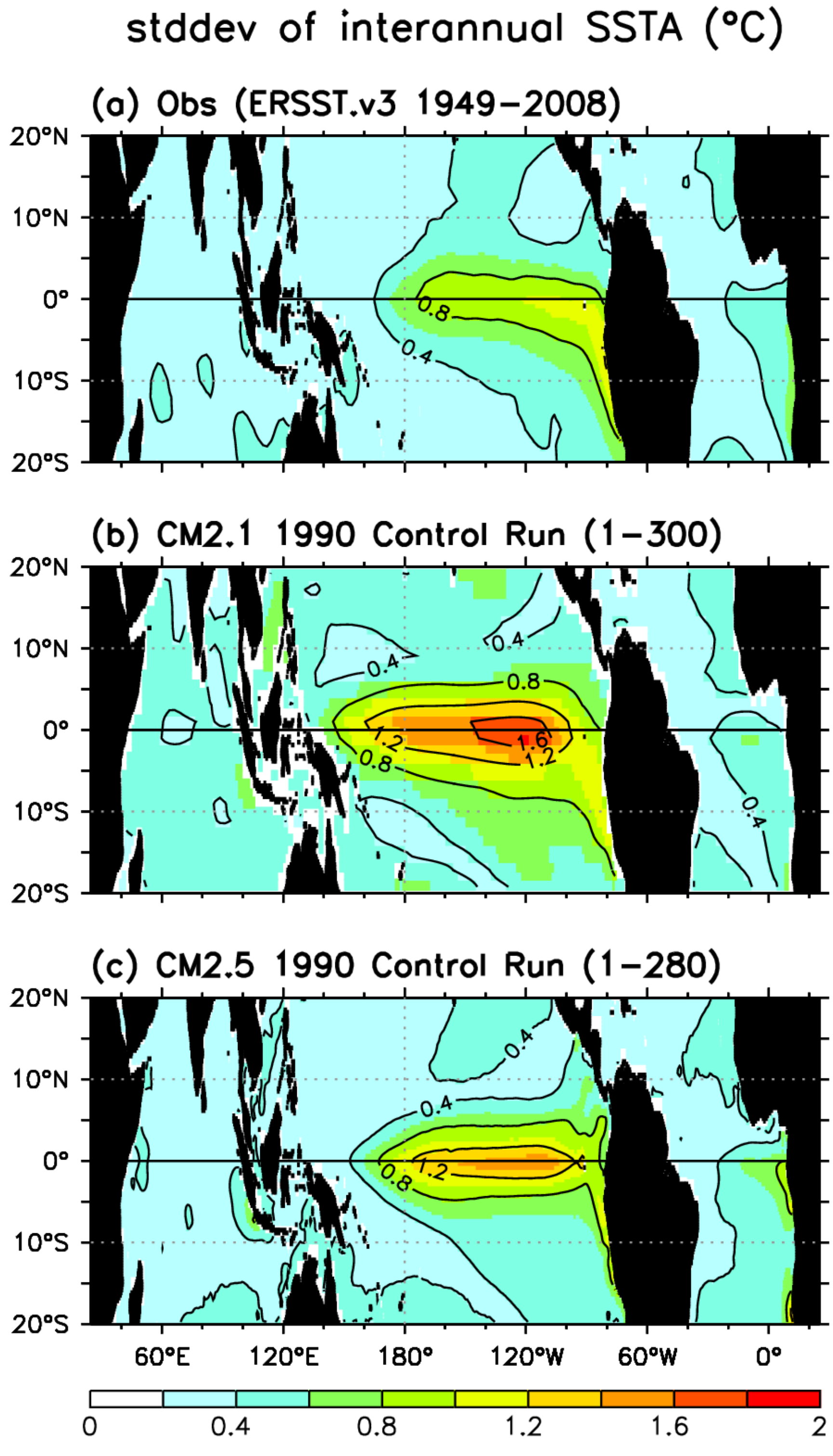

Figure 15 Standard deviation of SST anomalies (°C) over the tropics, after applying a 9-month triangle smoother that transmits (25, 50, 75)% of the time series amplitude at periods of (8, 11, 17) months. (a) Observations from the Smith et al, 2008, years 1949-2008; (b) CM2.1 1990 control run, years 1-300; (c) CM2.5 1990 control run, years 1-280. Note that in contrast to many of the other analyses in this paper, we use the full length of the model experiments to characterize ENSO related variability.

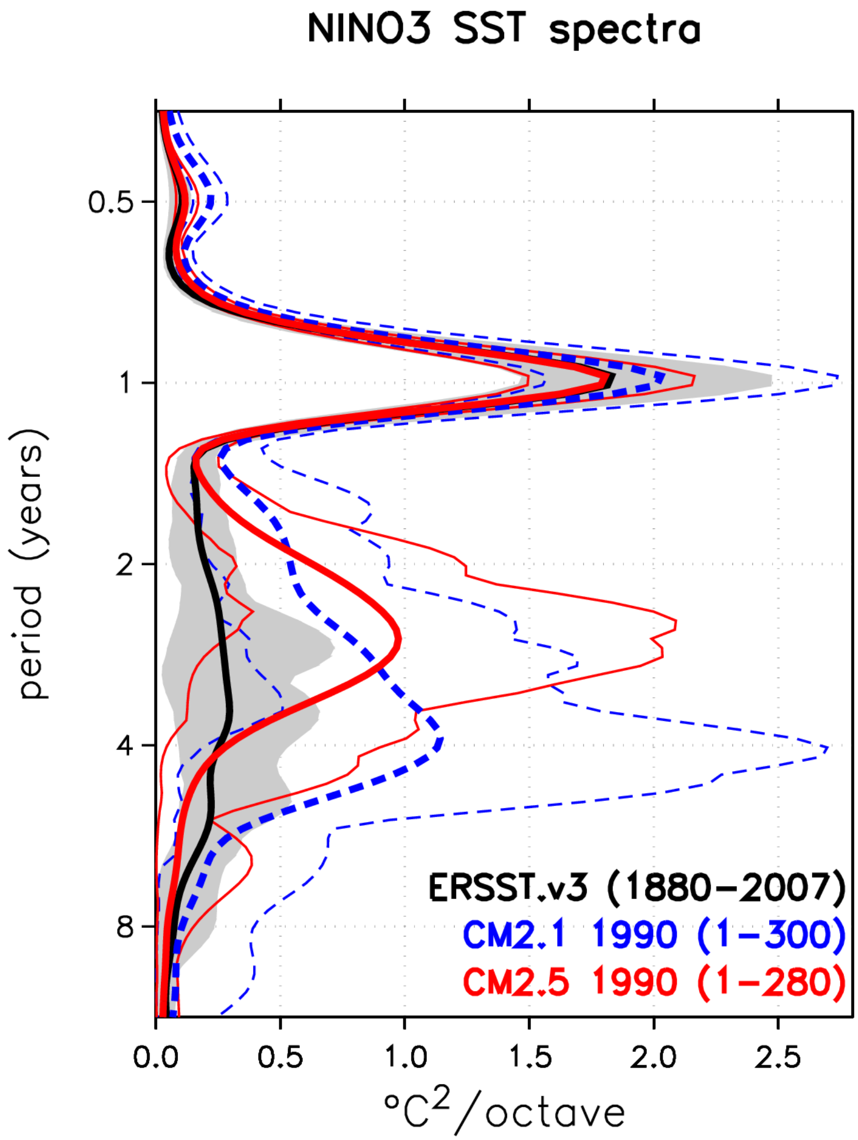

Fig. 16 (a) Spectral power (°C^2 octave^{-1}) of NINO3 SSTs, as a function of period in octaves of the annual cycle, computed by time-averaging the spectral power density from a Morlet wavenumber-6 wavelet analysis. The area to the left of each curve represents the spectral power within a frequency band. Thick black line is the observed 128-yr-mean spectrum for 1880-2007, from ERSST.v3 (Smith et al. 2008). Thick blue dashed (red solid) line is the 300-yr-mean (280-yr mean) spectrum from years 1-300 (1-280) of the CM2.1 (CM2.5) 1990 control run. Gray shading (thin lines) indicate the min/max range of sliding 20-yr-mean spectra from the observed (simulated) time series.

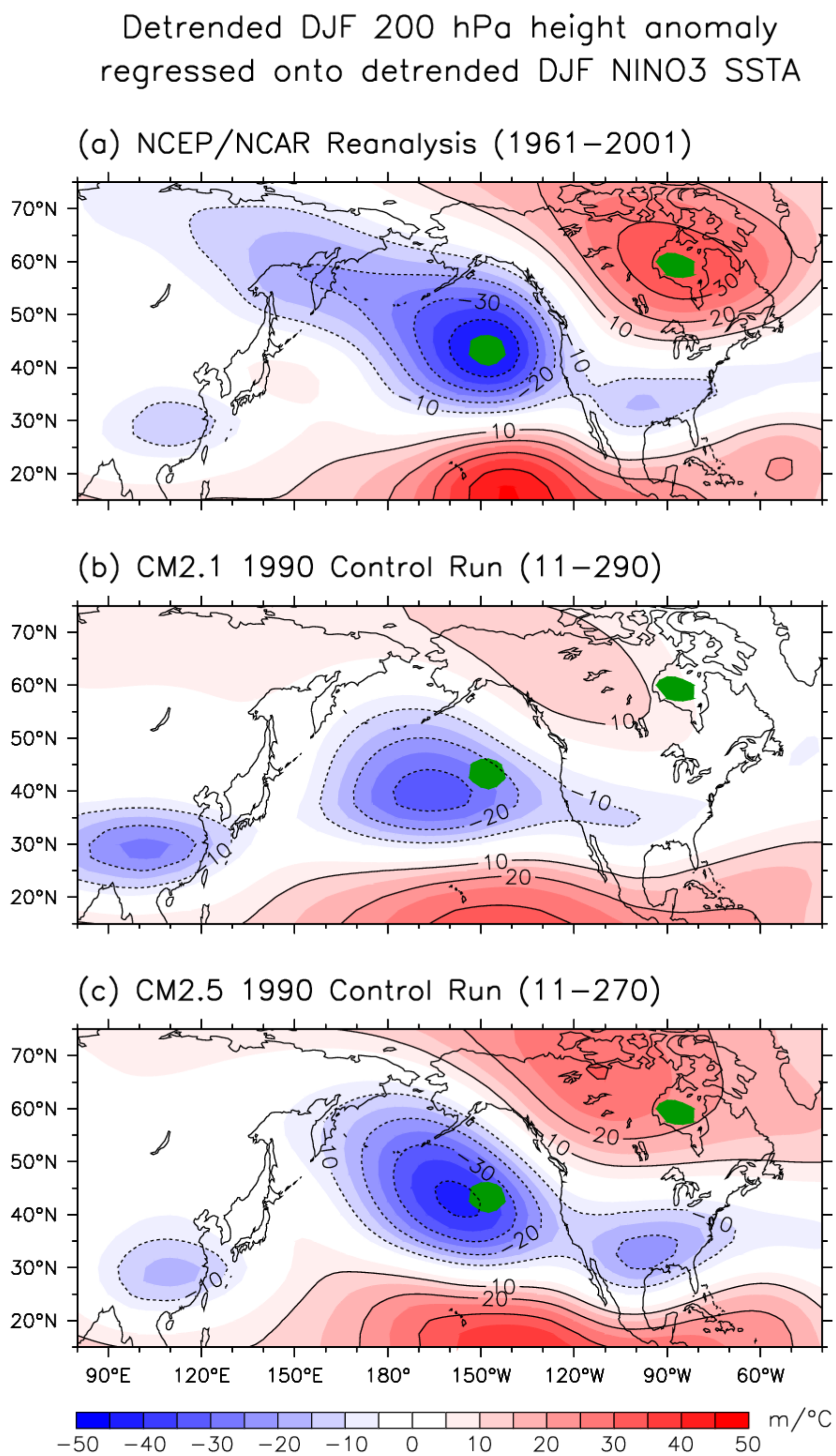

Figure 17 DJF 200-hPa geopotential height anomalies regressed onto DJF NINO3 SSTAs, computed using (a) the NCEP/NCAR Reanalysis (Kistler et al. 2001) for 1961-2001; (b) the CM2.1 1990 control run for years 11-290; (c) the CM2.5 1990 control run for years 11-270. The zero contour is omitted. Green shading in all panels indicates the positions of the observed extrema over the North Pacific and Canada. Prior to computing the seasonal anomalies and regressions, all time series were detrended by removing a 20-yr running mean.

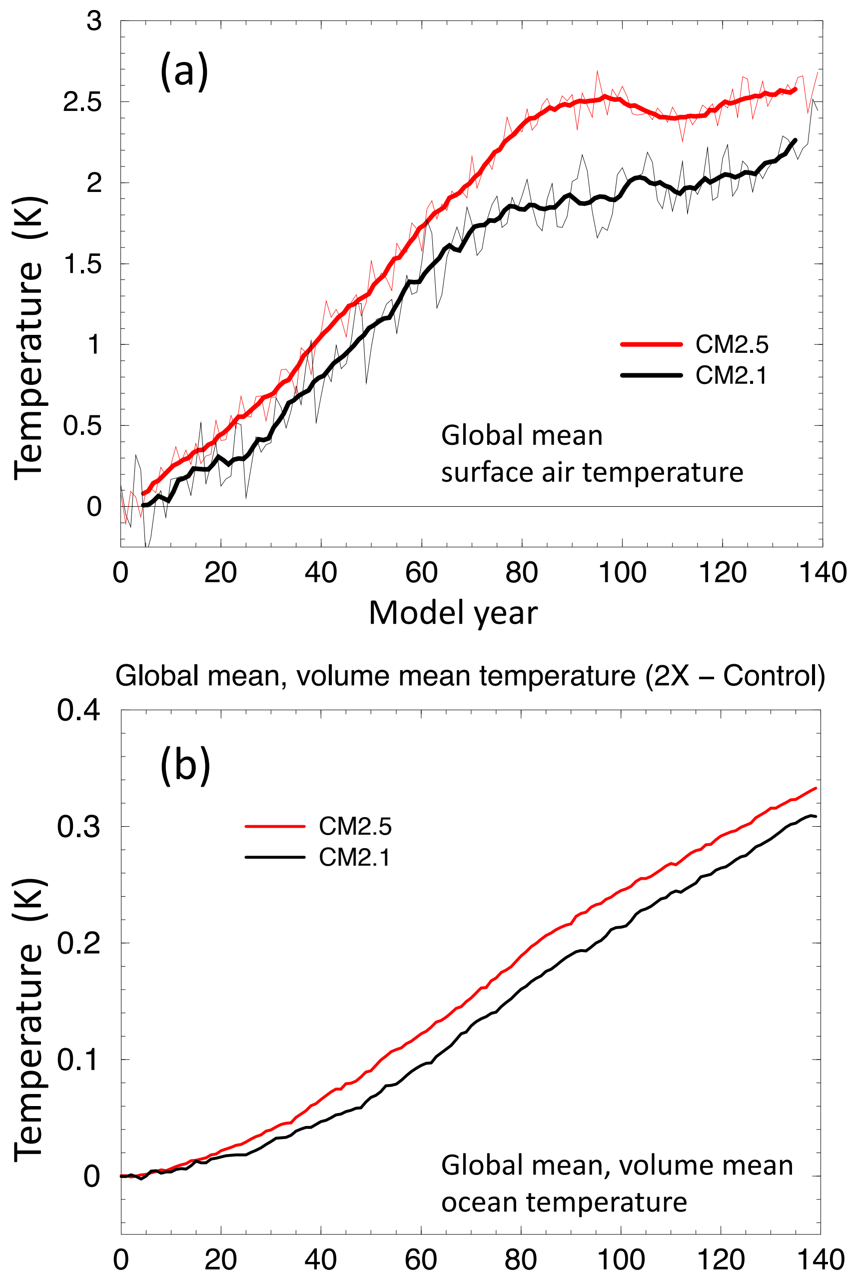

Figure 18 (a) Time series of response of global-mean near-surface air temperature to increasing atmospheric CO_2. Annual mean temperature responses are plotted, calculated as temperature from the 2X CO_2 runs minus temperature from a corresponding section of the Control runs. Thin lines indicate annual means (black for CM2.1, red for CM2.5), while thick lines indicate 10 year low-pass filtered time series (black for CM2.1, red for CM2.5). (b) Global mean, volume mean ocean temperature change, 2X CO_2 experiment minus Control. Black curve for CM2.1, red curve for CM2.5.

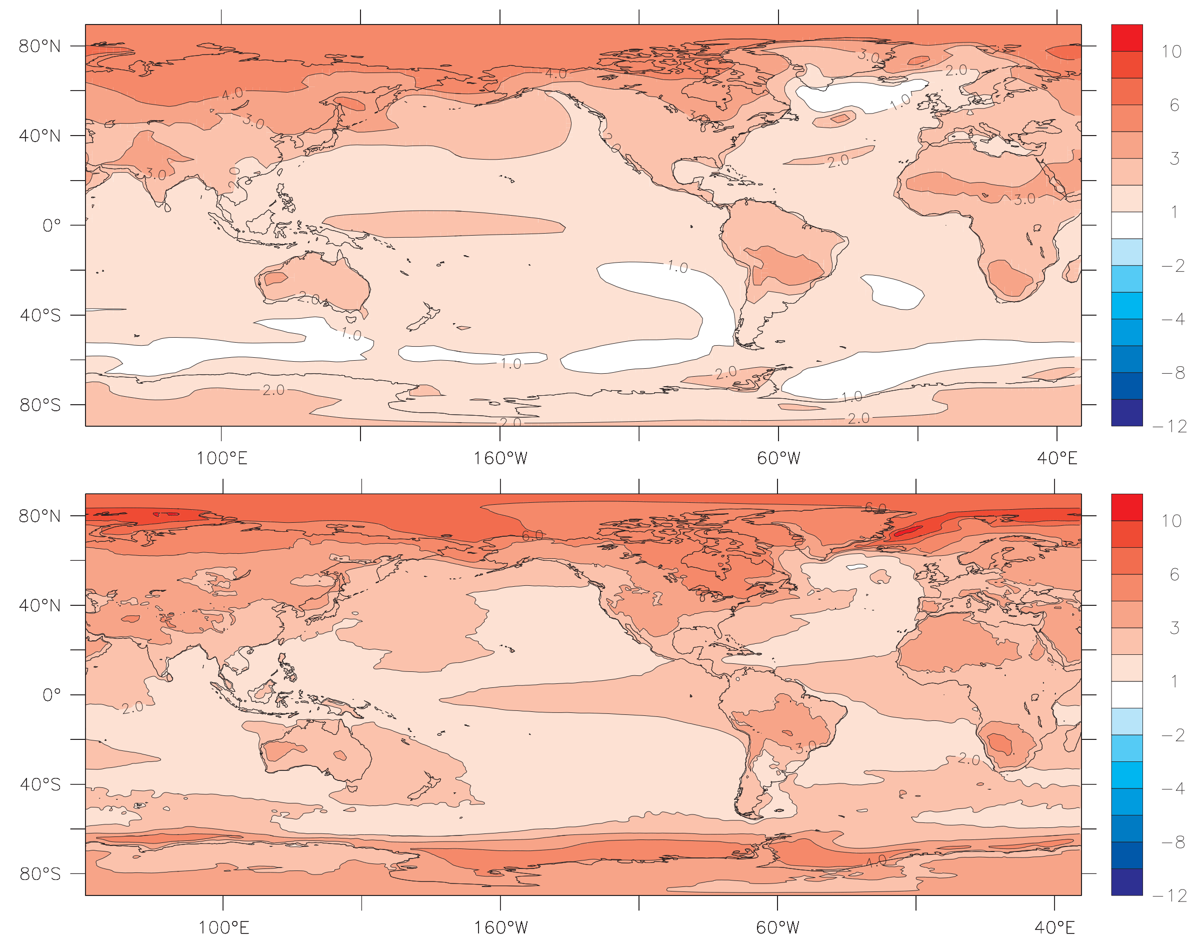

Figure 19 Map of change in annual-mean near-surface air temperature in response to increasing CO_2. Maps are computed using data averaged over years 91-140 of the 2X CO_2 runs minus the corresponding sections of the Control runs. Units are K. (a) CM2.1, (b) CM2.5.

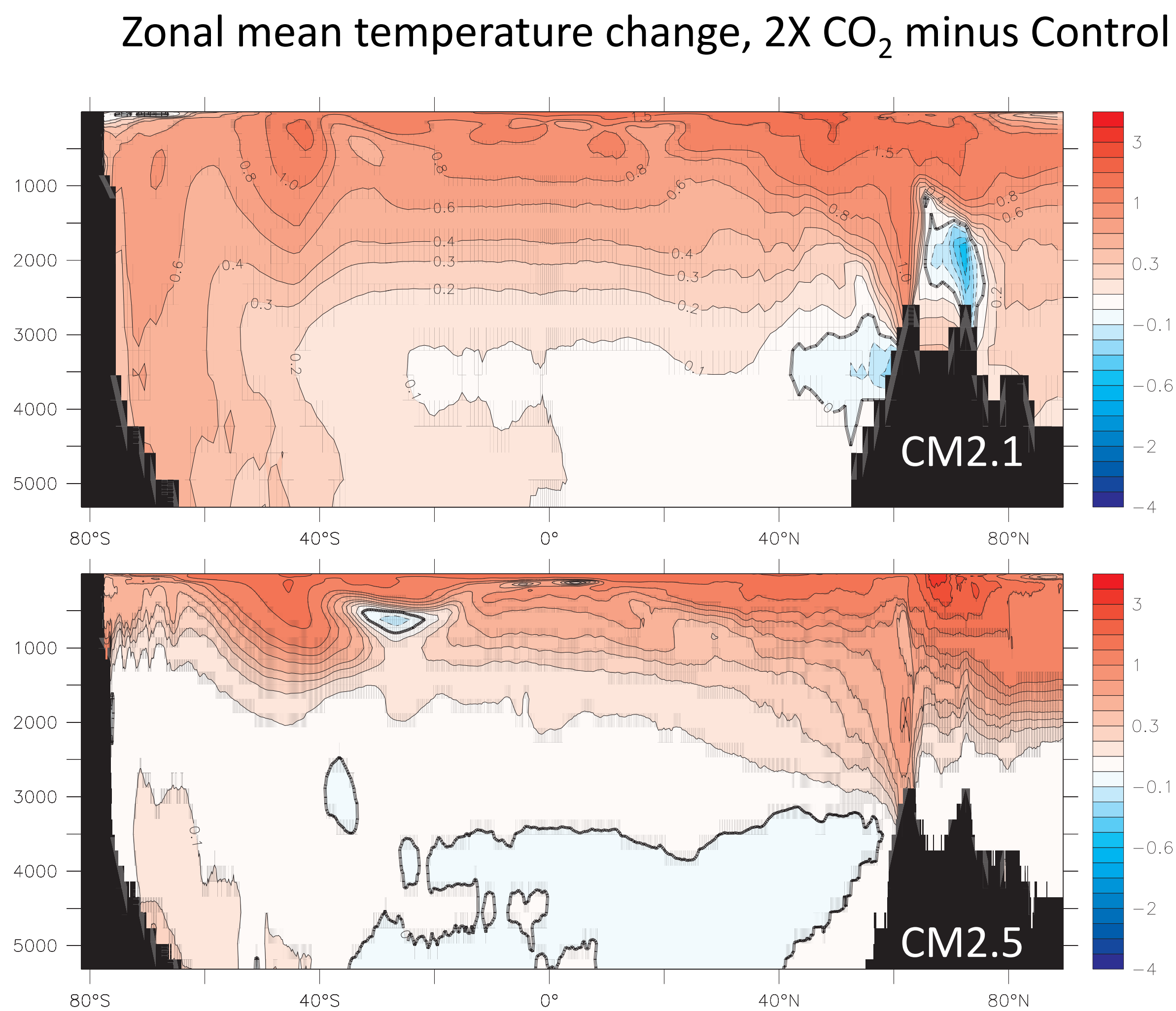

Figure 20 (a) Zonal mean of temperature change for model CM2.1 between 2X experiment and control run, computed as time mean of temperature in years 91-140 of the 2X experiment minus the corresponding section of the control. (b) Same for model CM2.5. Units are K.

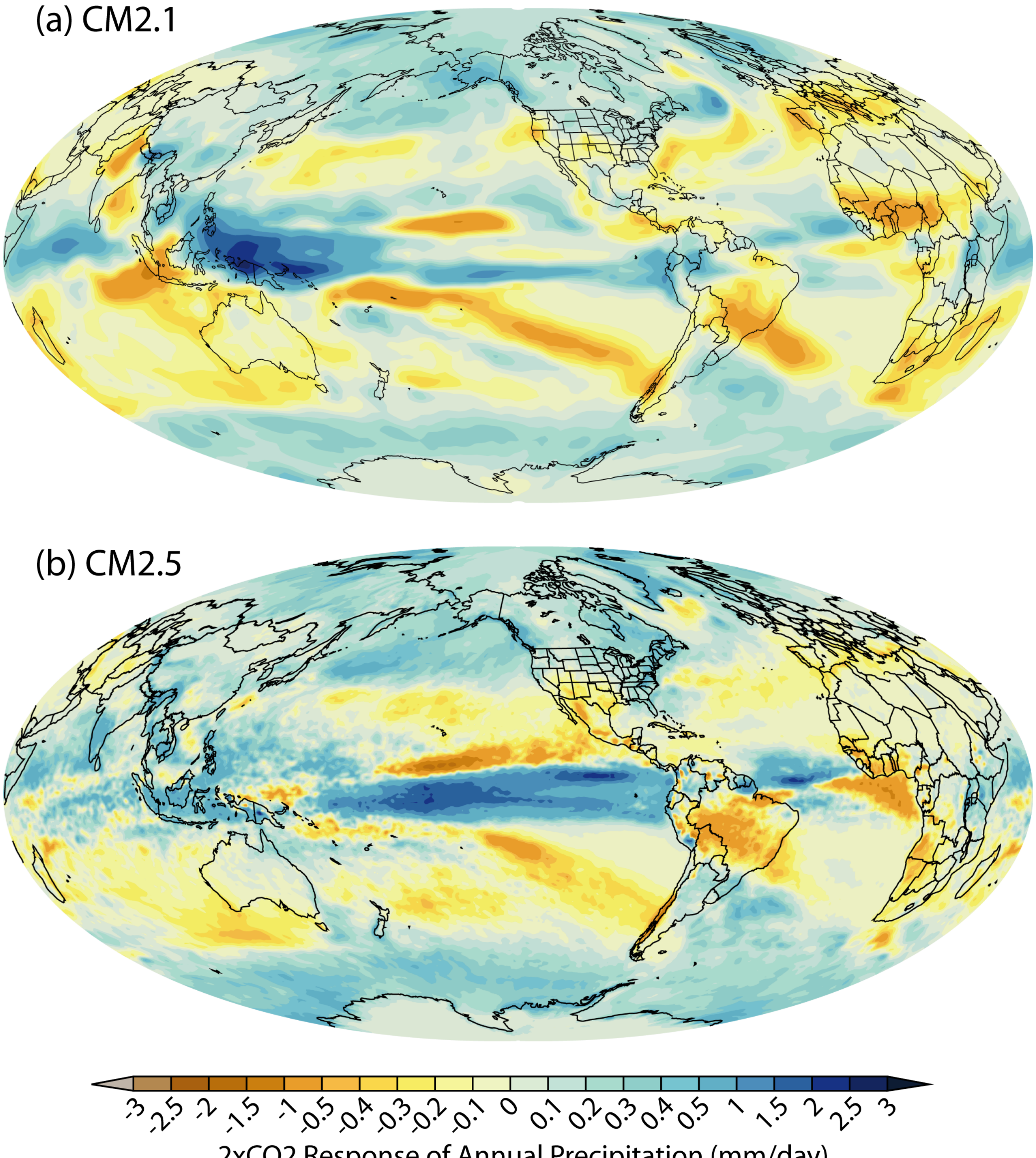

Figure 21 Map of change in annual-mean precipitation in response to increasing CO_2. Units are mm day^{-1}. Maps are computed using data averaged over years 91-140 of the 2X CO_2 runs minus the corresponding sections of the Control runs. (a) CM2.1, (b) CM2.5.

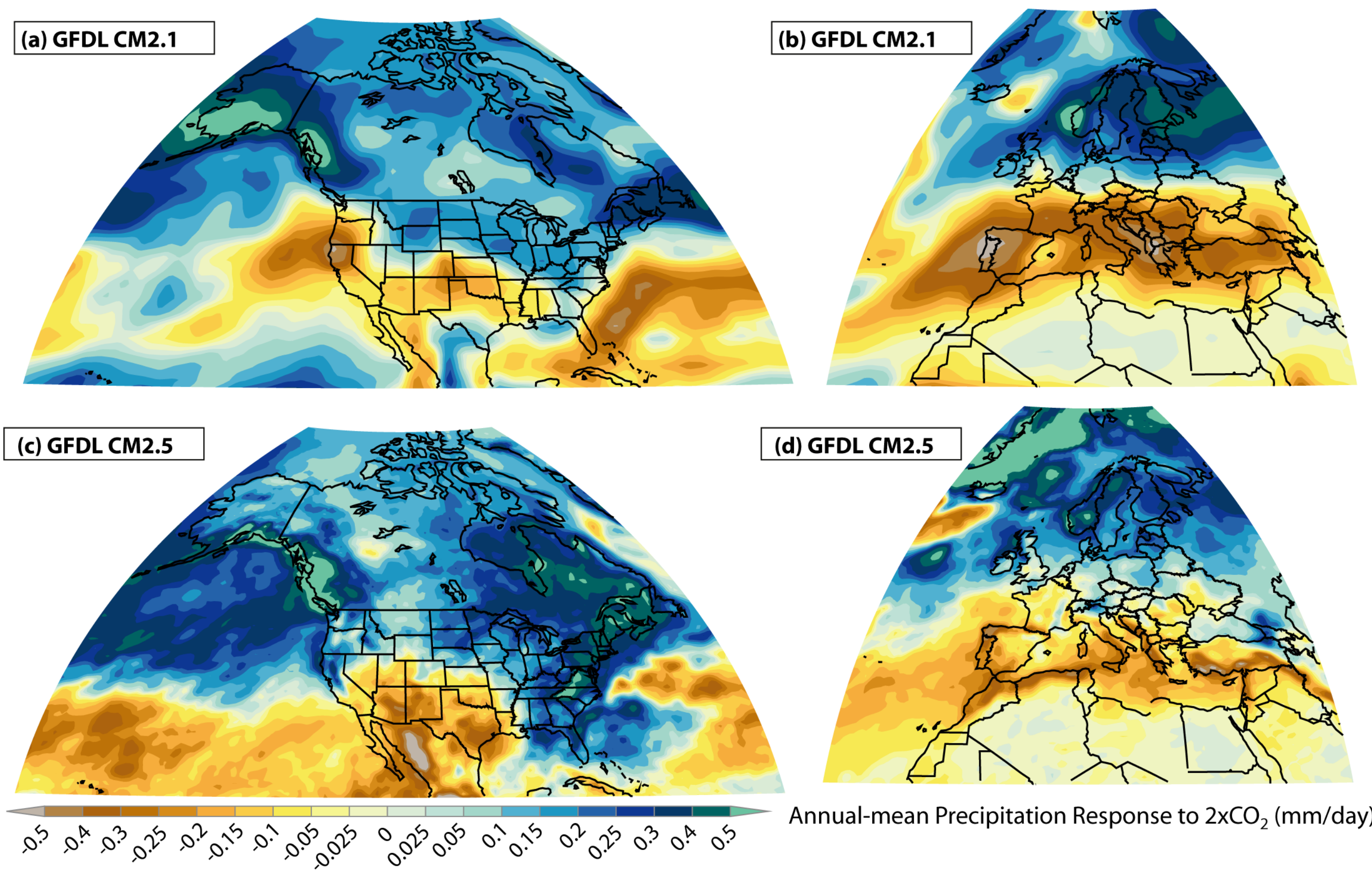

Figure 22 Map of change in annual-mean precipitation in response to increasing CO_2. Units are mm day^{-1}. Maps are computed using data averaged over years 91-140 of the 2X CO_2 runs minus the corresponding sections of the Control runs. (a) CM2.1 over North America, (b) CM2.1 over Europe and northern Africa, (c) CM2.5 over North America, (d) CM2.5 over Europe and northern Africa.

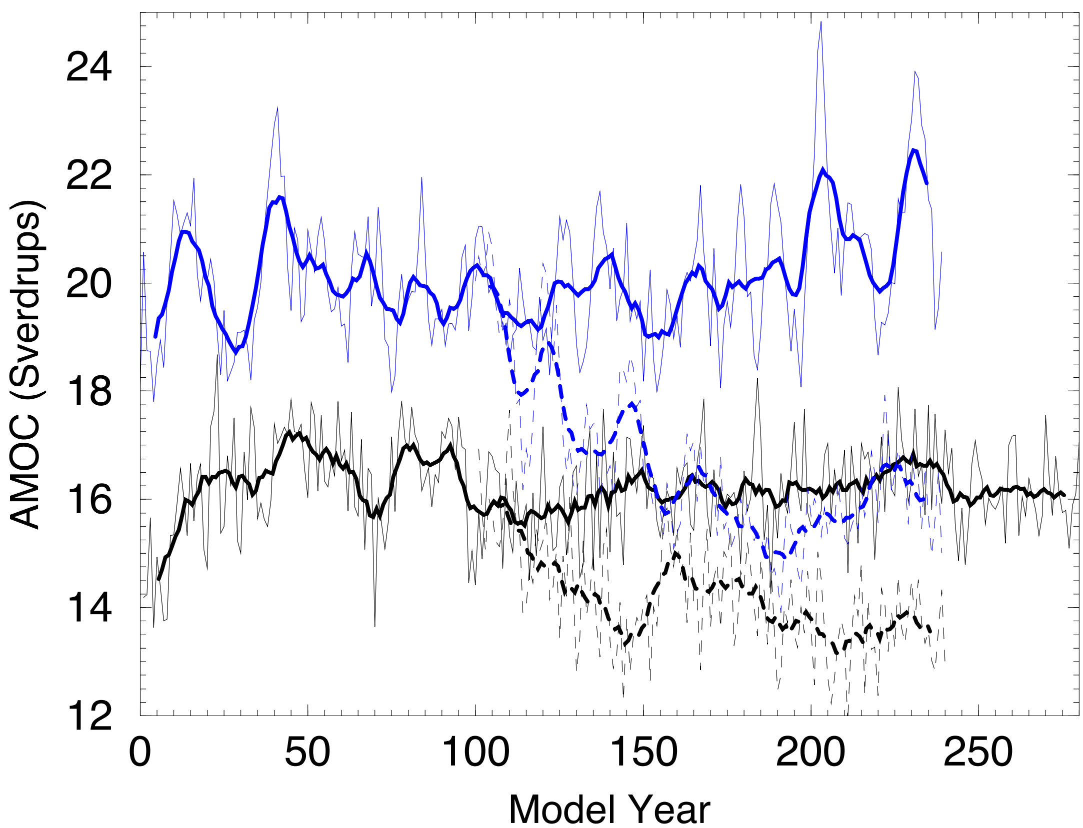

Figure 23 Time series of the AMOC index for various experiments; the index value is defined as the maximum value in the vertical of the annual mean AMOC field between 20^0N and 65^0N. Thin lines indicate annual mean values, while thick lines are 10 year running mean time series. Solid black indicates Control simulation from CM2.5, while dashed black indicates 2X CO_2 simulation from CM2.5. Solid blue indicates 1990 Control simulation from CM2.1, while dashed blue indicates 2X CO_2 simulation from CM2.1.